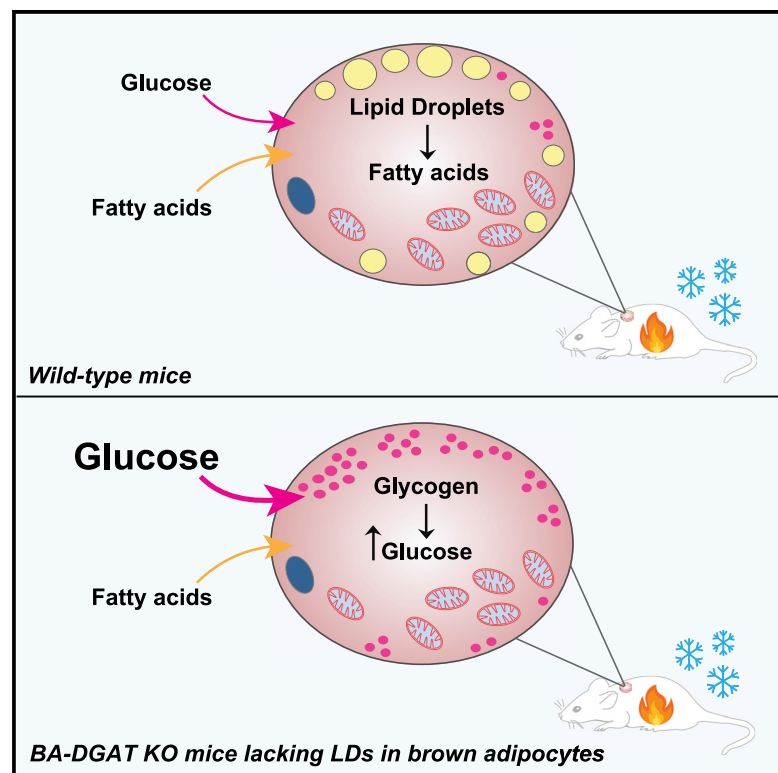


# Lipid Droplets in Brown Adipose Tissue Are Dispensable for Cold-Induced Thermogenesis

## Graphical Abstract



## Authors

Chandramohan Chitraju,  
Alexander W. Fischer,  
Robert V. Farese, Jr., Tobias C. Walther

## Correspondence

robert@hsph.harvard.edu (R.V.F.),  
twalther@hsph.harvard.edu (T.C.W.)

## In Brief

Chitraju et al. show that mice lacking triglycerides and lipid droplets in brown adipocytes maintain eutheria during acute or chronic cold exposure by using circulating glucose and fatty acids and stored glycogen to fuel thermogenesis.

## Highlights

- Lipid droplets are absent in brown adipocytes of mice lacking both DGAT1 and DGAT2
- Mice lacking lipid droplets in brown adipocytes maintain eutheria during cold exposure
- Brown adipocytes lacking lipid droplets use glucose, FAs, and glycogen as fuels
- Mice lacking triglycerides in brown adipocytes are resistant to glucose intolerance



## Report

# Lipid Droplets in Brown Adipose Tissue Are Dispensable for Cold-Induced Thermogenesis

Chandramohan Chitraju,<sup>1,2</sup> Alexander W. Fischer,<sup>1,2</sup> Robert V. Farese, Jr.,<sup>1,2,3,5,\*</sup> and Tobias C. Walther<sup>1,2,3,4,5,6,\*</sup><sup>1</sup>Department of Molecular Metabolism, Harvard T.H. Chan School of Public Health, Boston, MA 02115, USA<sup>2</sup>Department of Cell Biology, Harvard Medical School, Boston, MA 02115, USA<sup>3</sup>Broad Institute of Harvard and MIT, Cambridge, MA 02142, USA<sup>4</sup>Howard Hughes Medical Institute, Boston, MA 02115, USA<sup>5</sup>These authors contributed equally<sup>6</sup>Lead Contact\*Correspondence: [robert@hsph.harvard.edu](mailto:robert@hsph.harvard.edu) (R.V.F.), [twalther@hsph.harvard.edu](mailto:twalther@hsph.harvard.edu) (T.C.W.)<https://doi.org/10.1016/j.celrep.2020.108348>**SUMMARY**

Brown adipocytes store metabolic energy as triglycerides (TGs) in lipid droplets (LDs). Fatty acids released from brown adipocyte LDs by lipolysis are thought to activate and fuel UCP1-mediated thermogenesis. Here, we test this hypothesis by preventing fatty acid storage in murine brown adipocytes through brown adipose tissue (BAT)-specific deletions of the TG synthesis enzymes DGAT1 and DGAT2 (BA-DGAT KO). Despite the absence of TGs in brown adipocytes, BAT is functional, and BA-DGAT-KO mice maintain euthermy during acute or chronic cold exposure. As apparent adaptations to the lack of TG, brown adipocytes of BA-DGAT-KO mice appear to use circulating glucose and fatty acids, and stored glycogen, to fuel thermogenesis. Moreover, BA-DGAT-KO mice are resistant to diet-induced glucose intolerance, likely because of increased glucose disposal by BAT. We conclude that TGs in BAT are dispensable for its contribution to cold-induced thermogenesis, at least when other fuel sources are available.

**INTRODUCTION**

Homeotherms maintain constant body temperature despite changes in ambient temperature. Mammals maintain core body temperature by adaptive thermogenesis, including shivering and non-shivering thermogenesis (Cannon and Nedergaard, 2004; Lowell and Spiegelman, 2000). In non-shivering thermogenesis, brown and brite/beige fat dissipates chemical energy as heat by uncoupling respiration from ATP synthesis (Shabalina et al., 2013; Smith and Roberts, 1964; Smith et al., 1966; Wu et al., 2012), as well as by other “futile” enzymatic cycles (Chouchani et al., 2019; Kazak et al., 2015).

Non-shivering thermogenesis is fueled by different energy sources, including triglycerides (TGs), glucose, fatty acids (FAs) (Bartelt et al., 2011; Cannon and Nedergaard, 2004; Townsend and Tseng, 2014), succinate (Mills et al., 2018), and branched-chain amino acids (Yoneshiro et al., 2019). In rodents, glucose is a major fuel, with ~20% of circulating glucose being consumed by brown adipose tissue (BAT) under basal conditions (Hankir and Klingenspor, 2018). With respect to FAs, cold exposure of mice activates the sympathetic nervous system, which leads to stimulation of adipose TG lipase (ATGL) activity by comparative gene identification-58 (CGI-58) (Lass et al., 2006). ATGL-mediated lipolysis of TGs stored in lipid droplets (LDs) of brown and white adipocytes liberates FAs that can be used as fuel (Schreiber et al., 2017; Shin et al., 2017; Zechner et al., 2012). In addition, FAs can be generated as a fuel source from TG-rich lipoproteins (Bartelt et al., 2011; Heine et al., 2018).

The requirement for storage of FAs as TGs in brown adipocytes for thermogenesis has not been strictly determined. Recent studies, deleting either ATGL or CGI-58 in murine BAT, showed that TG lipolysis catalyzed by ATGL in brown adipocytes is not required for mice to maintain body temperature during cold exposure (Schreiber et al., 2017; Shin et al., 2017), suggesting that FAs stored in brown adipocytes are not needed to fuel thermogenesis. However, hormone-sensitive lipase (HSL) can also catalyze TG hydrolysis (Schweiger et al., 2006) and may have compensated for the loss of ATGL in these studies (Schreiber et al., 2017; Shin et al., 2017).

Here we sought to determine whether TG storage in LDs of murine brown adipocytes is required for thermogenesis and euthermy. To address this, we generated mice lacking TGs in BAT by deleting both acyl CoA:diacylglycerol acyltransferase (DGAT) enzymes, DGAT1 and DGAT2 (Cases et al., 1998, 2001; Yen et al., 2008), specifically in BAT (BA-DGAT knockout [KO]). We then studied the physiology of these mice in response to thermogenic challenges.

**RESULTS****TG Stores and LDs Are Absent in Brown Adipocytes of Mice Lacking Both DGAT1 and DGAT2**

To generate BAT-specific *Dgat1* and *Dgat2* double-KO (BA-DGAT-KO) mice, we first generated *Dgat1* and *Dgat2* double-floxed mice (D1D2 flox) by crossing *Dgat1*<sup>flox/flox</sup> mice (Shih et al., 2009) with *Dgat2*<sup>flox/flox</sup> mice (Chitraju et al., 2019). We then crossed D1D2 flox mice with transgenic mice expressing



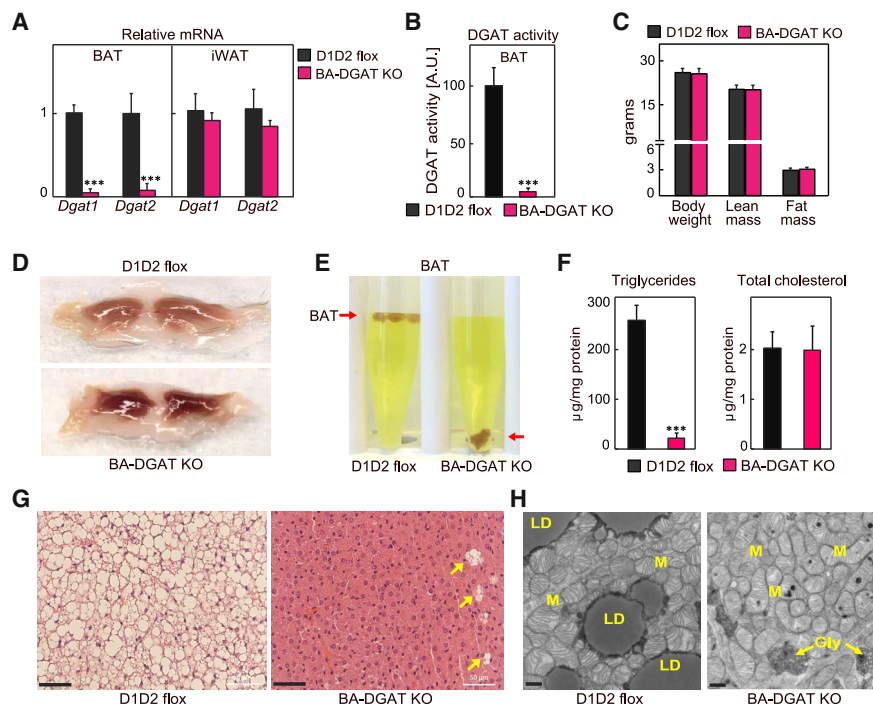


**Figure 1. Triglycerides and Lipid Droplets (LDs) Are Absent in BAT of BA-DGAT-KO Mice**

Brown adipose tissue-specific *Dgat1* and *Dgat2* double-knockout mice (BA-DGAT KO) were generated by crossing D1D2 flox mice with mice expressing the Cre-recombinase under control of the *Ucp1* promoter.

(A) mRNA levels of *Dgat1* and *Dgat2* in BAT and iWAT (n = 6).

(B) DGAT activity in BAT lysates (n = 4).

(C) Lean mass and fat mass analysis of 10-week-old chow diet-fed mice (n = 8).

(D) Gross appearance of interscapular BAT.

(E) BAT of BA-DGAT-KO mice sinks in an aqueous buffer with fixative (1.25% formaldehyde, 2.5% glutaraldehyde, and 0.03% picric acid in 0.1 M sodium cacodylate buffer, pH 7.4, density = 1.01 g/mL) used to fix BAT tissue for electron microscopy.

(F) Triglycerides and total cholesterol content in BAT (n = 5).

(G) H&E-stained sections of BAT. LDs were absent in nearly all cells of BAT depots in BA-DGAT-KO mice. A few cells of unknown identity (arrowheads) in BAT of BA-DGAT-KO mice had LDs. Scale bars, 50 µm.

(H) Transmission electron microscopy (TEM) images of BAT. Scale bars, 2 µm. LD, lipid droplet; M, mitochondria; Gly, glycogen.

Data are presented as mean ± SD. \*\*\*p < 0.001, t test.

Cre recombinase under control of the murine *Ucp1* promoter (Kong et al., 2014).

BA-DGAT-KO mice were healthy and yielded offspring with the predicted Mendelian ratio of genotypes. *Dgat1* and *Dgat2* mRNA levels were decreased by ~95% and ~85%, respectively, in interscapular BAT of BA-DGAT-KO mice but were similar in inguinal white adipose tissue (iWAT) (Figure 1A). DGAT activity, measured in *in vitro* assays, was decreased by ~95% in BAT of BA-DGAT-KO mice (Figure 1B). Dual-energy X-ray absorptiometry (DEXA) analysis showed that BA-DGAT-KO mice and control D1D2 flox mice had similar fat and lean mass overall (Figure 1C), which was also reflected in experiments with nuclear magnetic resonance imaging (Figure S1A). Weights of gonadal white adipose tissue (WAT) depots (Figure S1B) were also similar in control D1D2 flox and BA-DGAT-KO mice. However, BAT from BA-DGAT-KO mice appeared darker than BAT from control mice (Figure 1D) and was more dense, sinking in an aqueous buffer with fixative (Figure 1E). Analysis of the lipids in the BAT-DGAT KO confirmed that TG stores in BAT were reduced by ~95%, whereas cholesterol levels were

normal (Figure 1F). Histological examination revealed that LDs were absent in nearly all cells of BAT in BA-DGAT-KO mice (Figure 1G). A few cells of unknown identity, which presumably do not express UCP1-Cre, in BAT of BA-DGAT-KO mice had LDs (Figures 1G and S1C). These cells may account for the little TG present in BAT of BA-DGAT-KO mice. Transmission electron microscopy (TEM) analyses verified that brown adipocytes of BA-DGAT-KO mice lacked LDs but had abundant mitochondria (Figure 1H).

Plasma analyses revealed that the levels of TGs were ~25% reduced in *ad libitum* fed BA-DGAT-KO mice (31 ± 4 versus 41 ± 8 mg/dL, p = 0.04) and glucose levels were slightly lower (146 ± 8 versus 158 ± 9 mg/mL, p = 0.01) than in control mice (Table S1). Plasma levels of free FAs, free glycerol, total cholesterol, and insulin were similar in the two groups of mice (Table S1).

### BA-DGAT-KO Mice Maintain Euthermia during Acute or Chronic Cold Exposure

To determine the contributions of TG stores in BAT to thermogenesis, we exposed BA-DGAT-KO mice to cold temperature.

In response to acute cold exposure (4°C) for 6 h with *ad libitum* feeding or for 5 h with fasting, BA-DGAT-KO mice maintained their core body temperature (Figure 2A). To further increase thermogenic demands and test whether TG stores are required for prolonged thermogenesis, we exposed mice to cold temperature for 1 week with *ad libitum* feeding. Again, we found no differences in core body temperatures between BA-DGAT-KO and control mice (Figure 2A). These results indicate that TG stores in BAT are dispensable for cold-induced thermogenesis in mice.

To better understand the metabolic physiology of BA-DGAT-KO mice, we performed indirect calorimetry. Basal rates of oxygen consumption, CO<sub>2</sub> production, and respiratory exchange ratio (RER) were normal in BA-DGAT-KO mice (Figures S2A–S2D). However, compared with control mice, BA-DGAT-KO mice exhibited a reduced increase in oxygen consumption and energy expenditure after administering CL 316,243, a β-3-adrenoceptor agonist that activates thermogenesis (Himms-Hagen et al., 1994) suggesting that BAT with TG stores has a higher respiratory capacity than BAT without lipid stores. Consistent with this interpretation, the RER of BA-DGAT-KO mice trended higher than controls after CL 316,243 treatment, suggesting BA-DGAT-KO mice use less fat or more glucose in response to this challenge (Figure S2C).

We hypothesized that brown adipocytes of BA-DGAT-KO mice use fuel sources other than BAT TGs to enable thermogenesis. Tissue glycogen levels were ~5-fold higher in BAT of BA-DGAT-KO mice housed at room temperature, and the excess glycogen was no longer apparent after 6 h of cold exposure (Figure 2B), suggesting that glycogen is a compensatory fuel. In agreement with this, we found moderate increases in the mRNA levels of glycogen synthase and glycogenin in BAT of BA-DGAT-KO mice (Figure 2C). Also, glycogen synthase activity was ~20% higher in BAT-lysates of BA-DGAT-KO mice (Figure 2D).

BAT can also use circulating glucose and FAs to fuel cold-induced thermogenesis (Cannon and Nedergaard, 2004; Townsend and Tseng, 2014). For example, FAs released from WAT can fuel BAT-mediated thermogenesis in the fasted state (Schreiber et al., 2017; Shin et al., 2017). FA levels were increased 2- to 3-fold in fasted control mice exposed to cold (Figure 2E) but not in fasted BA-DGAT-KO mice, possibly because circulating FAs were being used for thermogenesis in BAT. Supporting this possibility, in tracer experiments ~40% less [<sup>14</sup>C]-oleic acid accumulated in BAT of BA-DGAT-KO mice compared with controls (Figure S2E), consistent with either reduced uptake or increased FA oxidation.

We next tested if glucose uptake by BAT was increased in BA-DGAT KO. [<sup>14</sup>C]-deoxyglucose uptake into BAT of BA-DGAT-KO mice was ~30% greater in the basal state or after treatment with CL 316,243 than in controls (Figure 2F). Similarly, <sup>18</sup>F-fluoro-deoxyglucose positron emission tomography/computed tomography scanning (<sup>18</sup>F-FDG-PET/CT) of mice after CL 316,243 injection showed that BAT of BA-DGAT-KO mice took up approximately 2-fold more glucose than BAT of control mice (Figure 2G).

These results prompted us to examine levels of glucose transporters in the BAT of BA-DGAT-KO mice. The mRNA expression of the glucose transporter *Glut1* was increased 2-fold in BAT of

BA-DGAT-KO mice, and *Glut4* mRNA levels were not changed (Figure 2C). GLUT1 and GLUT4 protein levels were similar in total homogenates of BAT from either genotype, but GLUT4 protein levels were ~40% higher in plasma membrane fractions isolated from BAT of BA-DGAT-KO mice compared with control levels (Figure 2H), suggesting increased translocation of GLUT4 to the plasma membrane.

We also investigated possible regulatory mechanisms underlying the increased glucose uptake in BA-DGAT-KO mice. On the basis of the phenotype associated with its murine KO, we considered lipocalin prostaglandin D synthase (L-PGDS); the activity of this enzyme has been implicated in fuel use by BAT, and L-PGDS-KO mice exhibit increased reliance on carbohydrate to provide fuel for thermogenesis (Virtue et al., 2012). Consistent with this, we detected a ~20% reduction in L-PGDS protein levels in BAT of BA-DGAT-KO mice compared with controls (Figure S2H), suggesting that reduced L-PGDS may be a contributing factor.

Glucose use in BAT is also regulated by β-3-adrenergic signaling through activation of AKT in an insulin-dependent manner (Heine et al., 2018; Sanchez-Gurmaches et al., 2018). However, we found normal levels of tyrosine hydroxylase, suggesting that β-3-adrenergic signaling was similar in BAT of BA-DGAT-KO and control mice (Figure 2I). Consistent with this, we also measured similar CL 316,243-stimulated phosphorylation of AKT (pAKT<sup>Ser473</sup>) in BAT of BA-DGAT-KO and control mice (Figure 2J). Also, phosphorylation of AKT (pAKT<sup>Ser473</sup>) was similar in BAT of BA-DGAT-KO and control mice after insulin treatment (Figure S2F). Thus, there were no apparent differences for AKT signaling in our model.

AMPK has also been implicated in regulating BAT glucose uptake by an insulin-independent mechanism (Teperino et al., 2012). We found a 10%–20% increase in pAMPK<sup>T172</sup> levels (top band in pAMPK blot) (Figure 2J) in BAT of BA-DGAT-KO mice, suggesting that AMPK may contribute to the increased plasma membrane localization of GLUT4.

### Adaptations of BAT Lacking TG Stores to Maintain Thermogenesis

Our results suggest that BAT lacking TG stores can compensate to fuel cold-induced thermogenesis by using alternative fuels, such as tissue glycogen, or glucose or FAs from the circulation. To determine how BAT of BA-DGAT-KO mice adapts, we examined changes in tissue gene expression. The mRNA levels of many BAT-specific and FA oxidation genes were similar in BAT of control and BA-DGAT KO-mice (Figure 3A), and mRNA levels of *Ucp1*, *Dio2*, and *Pgc1α* and FA oxidation genes increased similarly with cold exposure in BAT of BA-DGAT-KO and control mice (Figures 3B and S3A).

We also examined the expression of genes of lipogenesis, which are paradoxically increased in BAT with acute cold exposure (Sanchez-Gurmaches et al., 2018). Indeed, we found substantially increased expression of *de novo* FA synthesis (e.g., *Chrebpβ*, *Acc*, *Fas*) and elongation (*Elovl3*) genes in BAT of BA-DGAT-KO mice, both at baseline and after cold exposure (Figures 3A and S3A). Notably, the expression of the Δ9 desaturase *Scd1* was markedly decreased in BAT of BA-DGAT-KO mice (Figures 3A and S3A).

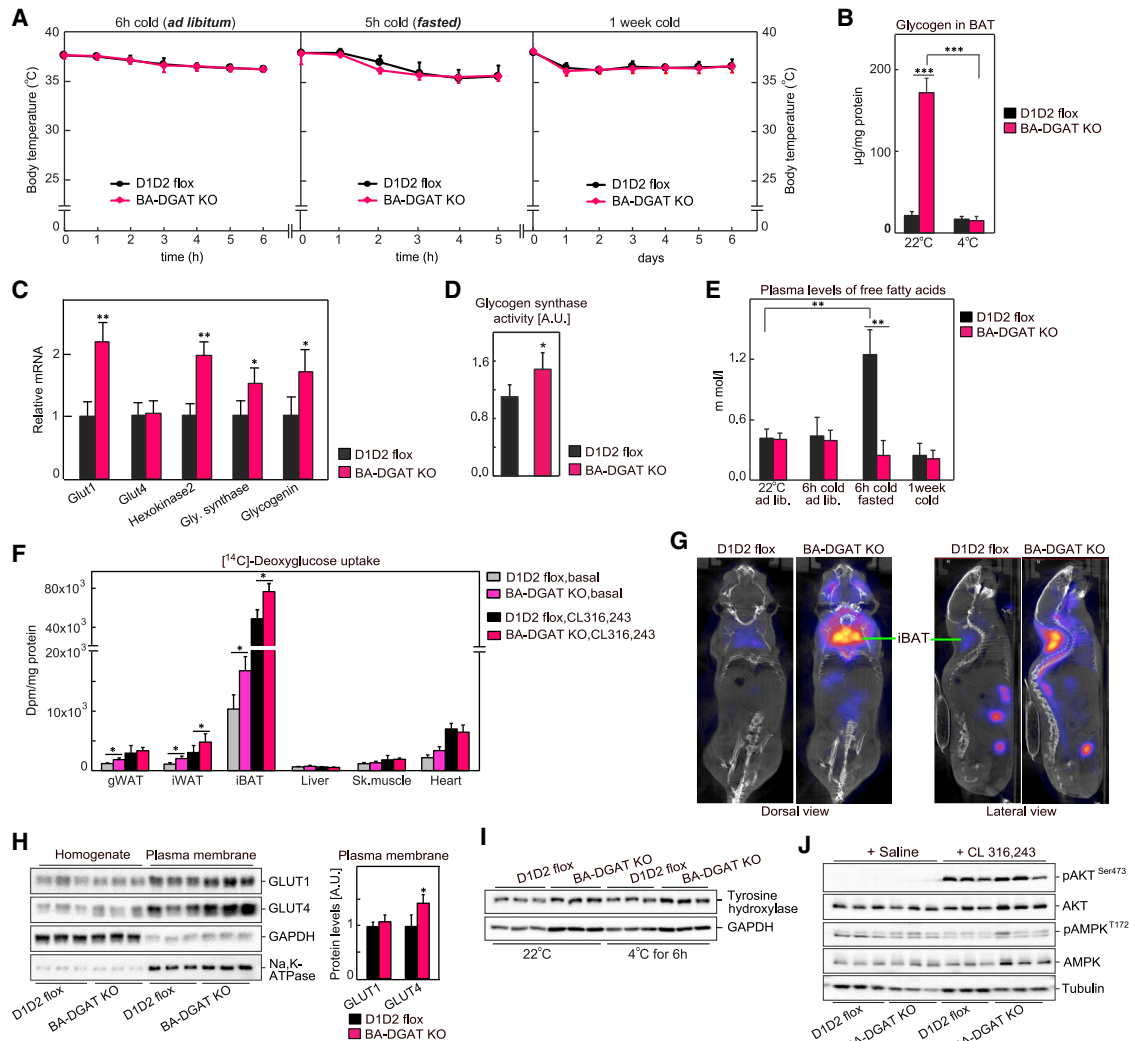


**Figure 2. BA-DGAT-KO Mice Maintain Euthermia during Acute or Chronic Cold Exposure**

(A) Mice were exposed to cold acutely (in *ad libitum* fed or in fasted state) or chronically for 1 week (n = 8).

(B) Glycogen levels in brown fat (n = 3).

(C) mRNA levels in BAT of mice housed at room temperature (n = 6).

(D) Glycogen synthase activity in BAT measured *in vitro* (n = 5).

(E) Plasma levels of free fatty acids (n = 7).

(F) [<sup>14</sup>C]-Deoxyglucose uptake by tissues *in vivo* in basal or CL 316,243-administered mice (n = 3).

(G) [<sup>18</sup>F]-FDG-PET/CT scans of CL 316,243-administered mice.

(H) Western blot analysis of glucose transporters in whole tissue homogenate and in plasma membrane fractions isolated from BAT of insulin-administered mice (n = 6).

(I) Western blot analysis of tyrosine hydroxylase in BAT of room temperature-housed or cold-exposed mice (n = 3).

(J) Western blot analysis of insulin signaling in BAT of basal or CL 316,243-administered mice (n = 3).

Data are presented as mean ± SD. \*p < 0.05, \*\*p < 0.01, and \*\*\*p < 0.001.

We also examined gene expression markers of endoplasmic reticulum (ER) stress and inflammation in BAT of BA-DGAT-KO mice. Sequestering FAs into TGs for storage in LDs protects white adipocytes from lipid-induced ER stress and lipotoxicity (Chitraju et al., 2017; Listenberger et al., 2003). We therefore expected that mice lacking TG storage might exhibit increased ER stress. However, expression of genes of the ER stress response were not increased in BAT of BA-DGAT-KO mice (Figures 3A and

S3A), consistent with the hypothesis that FAs were being oxidized and not accumulating in brown adipocytes.

We considered other adaptations in brown adipocytes of BA-DGAT-KO mice, such as changes in mitochondrial metabolism. Mitochondrial morphology, as assessed by EM, appeared to be normal in brown adipocytes of BA-DGAT-KO mice (Figure 1H). Total protein levels were similar in mitochondrial fractions isolated from BAT of BA-DGAT-KO and control mice

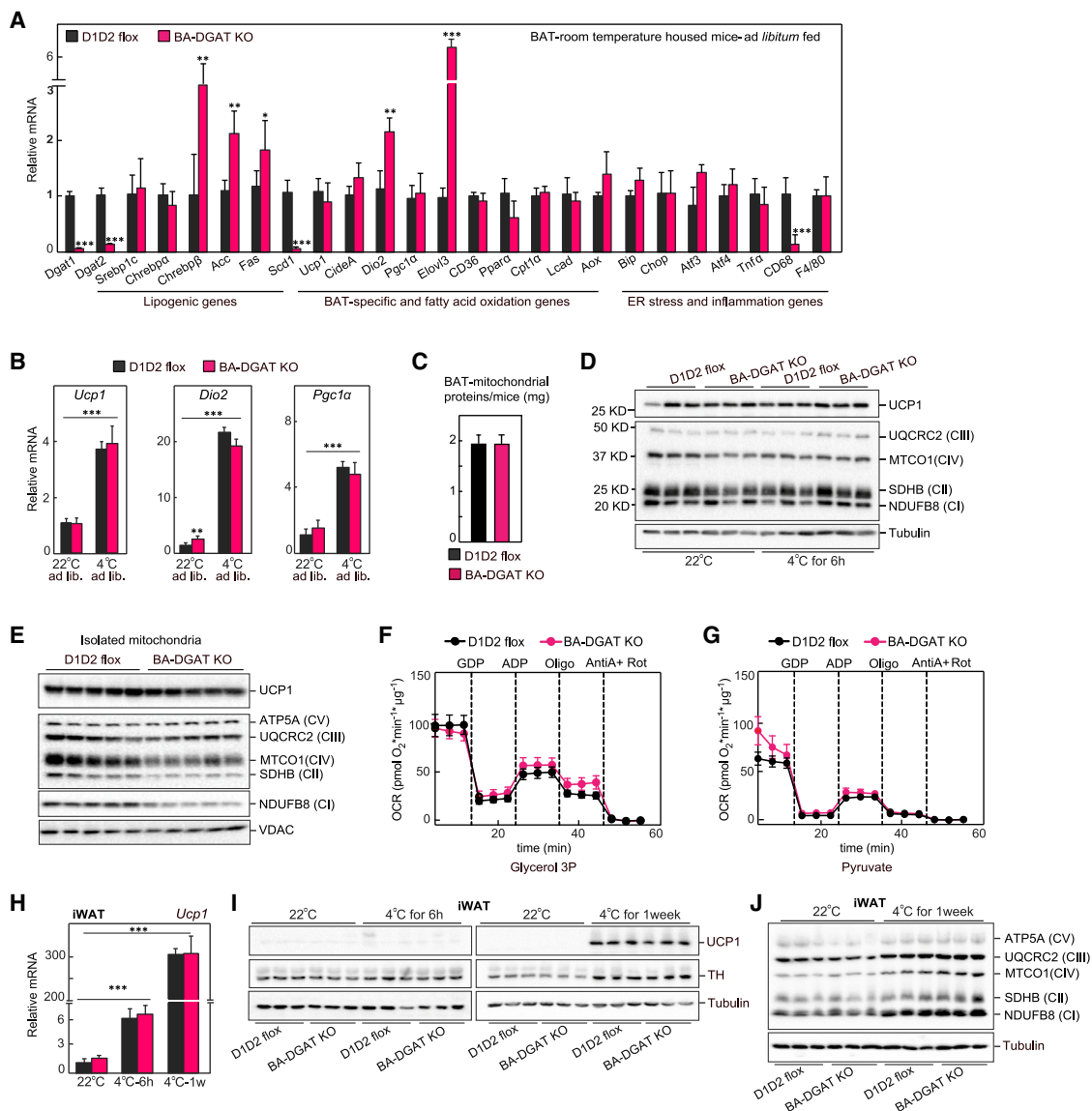


**Figure 3. Adaptations of BAT Lacking TG Stores to Maintain Thermogenesis**

(A) mRNA levels in BAT of mice housed at room temperature (n = 6).  
 (B) mRNA levels in BAT of *ad libitum* fed or cold-exposed (fasted) mice (n = 6).  
 (C) Total protein content of isolated mitochondria (n = 8).  
 (D) Western blot analysis of mitochondrial proteins from BAT tissue lysates (n = 4).  
 (E) Western blot analysis of mitochondrial proteins from isolated mitochondria (n = 4).  
 (F and G) Oxygen consumption rates (OCR) of isolated mitochondria measured using glycerol-3-phosphate or pyruvate as substrates. The difference between initial respiration and respiration after GDP addition was considered UCP1 activity. The difference between respiration after ADP addition and after oligomycin addition was considered ATP synthase activity (n = 4).  
 (H) mRNA levels of *Ucp1* in iWAT of room temperature-housed or acutely cold-exposed mice (n = 6).  
 (I) Western blot analysis of UCP1 and tyrosine hydroxylase (TH) in iWAT of room temperature-housed or cold-exposed mice (n = 3).  
 (J) Levels of OXPHOS proteins in iWAT of room temperature-housed or cold-exposed mice (n = 3).  
 Data are presented as mean  $\pm$  SD. \*p < 0.05, \*\*p < 0.01, and \*\*\*p < 0.001.

(Figure 3C). UCP1 protein levels in whole BAT tissue lysates and in isolated mitochondria of BA-DGAT-KO mice were also normal (Figures 3D and 3E). Western blot analysis of respiratory complex proteins showed similar levels of proteins in whole BAT tissue lysates (Figure 3D). NDUFB8 (complex I) and SDHB (com-

plex II) levels were mildly reduced in isolated mitochondria of BA-DGAT-KO mice (Figure 3E). However, we found similar levels of UQCRC2 (complex III) and ATP5A (complex V) (Figure 3E).

To test whether the changes in mitochondrial proteins affect mitochondrial respiration, we isolated mitochondria from BAT

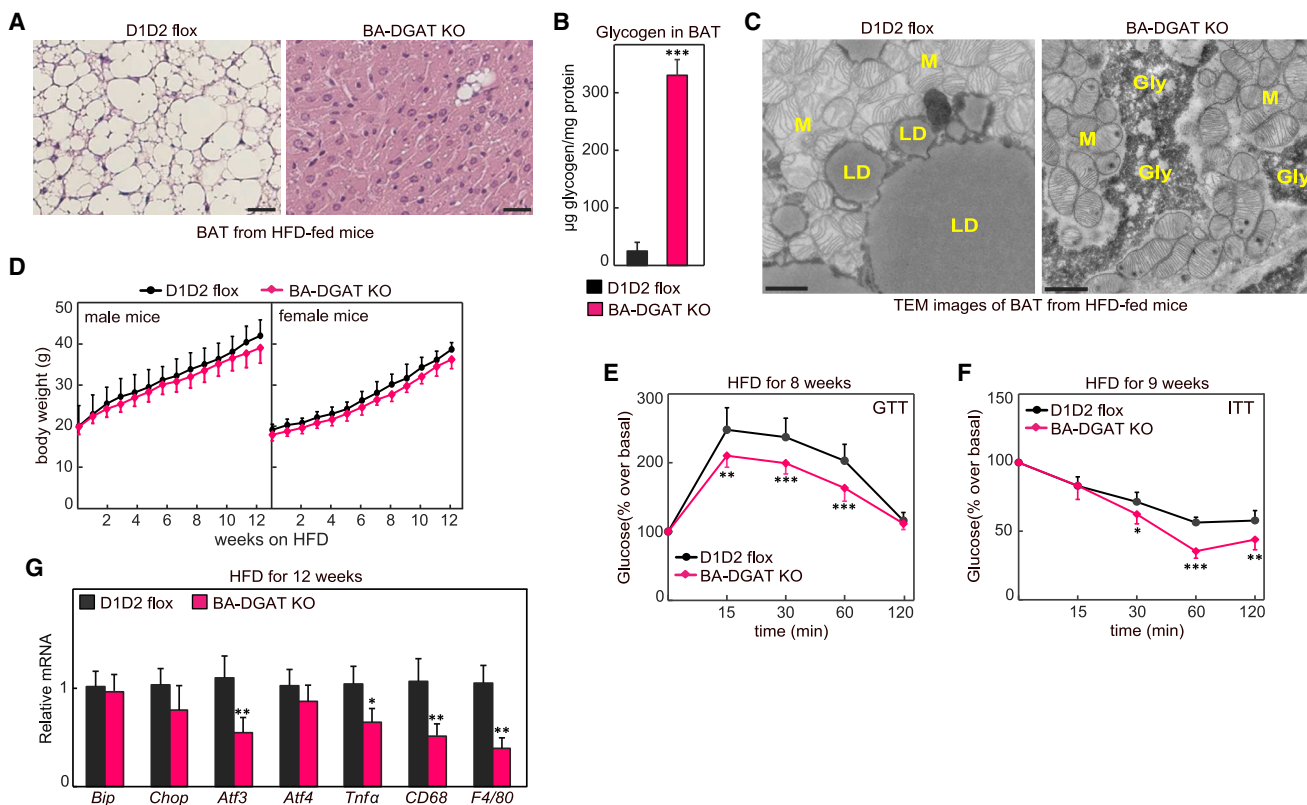


**Figure 4. BA-DGAT-KO Mice Are Resistant to High-Fat Diet (HFD)-Induced Glucose Intolerance**

(A) H&E-stained sections of BAT from 12-week HFD-fed mice; scale bars, 25  $\mu$ m.

(B) Glycogen levels in BAT of HFD-fed mice (n = 3).

(C) TEM images of BAT from HFD-fed mice. Scale bars, 2  $\mu$ m. LD, lipid droplet; M, mitochondria; Gly, glycogen.

(D) Body weights of mice fed on Western-type HFD (n = 15).

(E and F) Glucose tolerance test and insulin tolerance test performed on HFD-fed mice (n = 10). The GTTs were performed on 16-h fasted mice, when the basal glucose level was  $125 \pm 8$  mg/dL in BA-DGAT-KO mice compared with  $136 \pm 9$  mg/dL in control mice ( $p = 0.016$ , unpaired two-tailed Student's t test). The ITTs were performed on 4-h fasted mice with basal glucose levels of  $160 \pm 6$  mg/dL in BA-DGAT-KO compared with  $181 \pm 10$  mg/dL in control mice ( $p = 0.001$ , unpaired two-tailed Student's t test).

(G) mRNA levels in BAT of HFD-fed mice (n = 6).

Data are presented as mean  $\pm$  SD. \* $p < 0.05$ , \*\* $p < 0.01$ , \*\*\* $p < 0.001$ , and \*\*\*\* $p < 0.000$ , two-way ANOVA with Bonferroni's multiple-comparison test (for E and F). \* $p < 0.05$ , \*\* $p < 0.01$ , and \*\*\* $p < 0.001$ , t test (for B and G).

and measured oxygen consumption rates (OCRs) in response to different substrates. The basal OCRs were similar in mitochondria isolated from BA-DGAT-KO and control mice with glycerol-3-phosphate or pyruvate as substrates (Figures 3F and 3G). Respiration with maximal ATP-synthase activity (ADP addition) was slightly reduced in mitochondria of BA-DGAT-KO mice. UCP1-dependent respiration (GDP-inhibitable) was similar in mitochondria of BA-DGAT-KO and controls with glycerol-3-phosphate or pyruvate as substrates (Figures 3F and 3G).

Taken together, these results suggest that although mitochondria of BAT of BA-DGAT-KO mice exhibit some changes in levels of OXPHOS complex proteins, they appear to have adapted to maintain relatively normal mitochondrial respiration.

#### Similar Beiging of Inguinal WAT of BA-DGAT-KO and Control Mice

To meet thermogenic demands, cold exposure induces beiging/browning of iWAT (Wu et al., 2012). We considered the possibility

that increased amounts of brite/beige adipocytes in WAT may have contributed to the maintenance of cold-induced thermogenesis in BA-DGAT-KO mice. To assess this, we measured mRNA and protein levels of thermogenic genes in iWAT. The mRNA levels of thermogenic genes, including *Ucp1*, *Pgc1 $\alpha$* , *Ppar $\alpha$* , *Lcad*, and *Mcad*, were similar in iWAT of acutely or chronically cold-exposed control or BA-DGAT-KO mice, as well as in high-fat diet (HFD)-fed mice (Figures 3H and S3C). UCP1 protein levels and respiratory complex proteins were also similar in iWAT of BA-DGAT-KO and control mice (Figures 3I and 3J). Together, these results suggest that cold-induced beiging of iWAT was similarly induced in BA-DGAT-KO and control mice.

#### BA-DGAT-KO Mice Are Resistant to HFD-Induced Glucose Intolerance

Given the increased glucose uptake into BAT of BA-DGAT-KO mice, we hypothesized that BA-DGAT-KO mice may have improved glucose tolerance under conditions that promote

insulin resistance. To test this hypothesis, we fed mice an HFD for 12 weeks. At the end of the study period, BAT from BA-DGAT-KO mice exhibited a phenotype similar to BAT of chow-fed BA-DGAT-KO mice, including a darker color (Figure S4A), higher density (Figure S4B), and near absence of LDs (Figure 4A). Also, a few cells of unknown identity in BAT of BA-DGAT-KO mice still had LDs (Figure 4A). Glycogen levels were ~10-fold higher in BAT of HFD-fed BA-DGAT-KO mice (Figure 4B). Glycogen granules were visible in electron microscopy images of BAT from HFD-fed BA-DGAT-KO mice (Figures 4C and S4C). As previous studies showed that DGAT-catalyzed TG synthesis is important to protect cells from high intracellular FA levels (Chitraju et al., 2017; Koliwad et al., 2010; Listenberger et al., 2003; Liu et al., 2014), we measured expression ER stress and inflammatory marker genes but found no increases (Figure 4G), possibly because of the increase consumption of potentially lipotoxic FAs for thermogenesis. Consistent with this possibility, free FA levels in BAT of HFD-fed BA-DGAT-KO mice were decreased compared with control mice (Figure S1D).

At the level of the whole animal, both control and BA-DGAT-KO mice gained similar amounts of weight on the HFD (Figure 4D). As BAT of BA-DGAT-KO mice consumes more glucose, we next tested whether these mice are resistant to diet-induced glucose intolerance. Glucose tolerance tests (GTTs) and insulin tolerance tests (ITTs) were performed on mice fed HFD for 8 and 9 weeks, respectively. The GTTs were performed on 16 h fasted mice, when the basal glucose levels were  $125 \pm 8$  mg/dL in BA-DGAT-KO mice compared with  $136 \pm 9$  mg/dL in control mice ( $p = 0.016$  by unpaired two-tailed Student's *t* test). The ITTs were performed on 4 h fasted mice with basal glucose levels of  $160 \pm 6$  mg/dL in BA-DGAT-KO mice compared with  $181 \pm 10$  mg/dL in control mice ( $p = 0.001$  by unpaired two-tailed Student's *t* test). In addition to these lower fasting glucose levels, we found that BA-DGAT-KO mice had enhanced glucose and insulin tolerance (Figures 4E and 4F), suggesting that their increased glucose uptake into BAT protects them from the impaired glucose metabolism normally found with this diet.

## DISCUSSION

By genetically deleting both DGAT enzymes in brown adipocytes, we show that TG storage in LDs of murine brown adipocytes is dispensable for thermogenesis in response to cold when other fuel sources are present. In the absence of TG stores in brown adipocytes, other substrates, such as circulating glucose and FAs, as well as increased brown adipocyte glycogen, appear to be sufficient to compensate to fuel respiration and thermogenesis. Analysis of mitochondria of brown adipocytes of BA-DGAT-KO mice showed that they were mostly functioning normally. Most of the changes in brown adipocytes of BA-DGAT-KO mice were in gene expression and suggest adaptations to generate long-chain saturated FAs, possibly for fuel or to drive uncoupling (Bertholet and Kirichok, 2019; Fedorenko et al., 2012). Notably, BA-DGAT-KO mice exhibited a reduced increase in energy expenditure after CL 316,243 administration, likely because of a lack of TG stores for hydrolysis. We found no evidence to implicate increased thermogenesis/being in iWAT (beyond levels in control mice) as a compensatory mech-

anism for the loss of TGs in BAT, although activation of alternative thermogenic mechanisms (Bertholet et al., 2017; de Meis, 2003; Kazak et al., 2015; Periasamy et al., 2017) in BA-DGAT-KO mice was not excluded.

Our findings agree with those showing that CGI-58-activated, ATGL-mediated lipolysis of stored TG in brown adipocytes is dispensable for cold-induced thermogenesis (Schreiber et al., 2017; Shin et al., 2017). A conclusion from these studies was that TG storage in brown adipocytes was likely not required for thermogenesis, provided that FAs could be derived from WAT stores. This appears also to be the case in our BA-DGAT-KO model, in which TGs are still present in WAT. The two models differ, however, as the BAT of BAT-ATGL-KO or BAT-CGI-58-KO mice still had TG stores that may be lipolyzed by HSL (Schweiger et al., 2006). Our model, in contrast, depletes TG stores in brown adipocytes and therefore definitively answers whether TG stores are required functionally.

The gene expression changes in BAT of BA-DGAT-KO mice suggest that one response to a lack of TG stores in this tissue is to activate *de novo* lipogenesis, even beyond what is normally found with cold exposure (Sanchez-Gurmaches et al., 2018). This pathway is chiefly regulated by SREBP and ChREBP transcription factors (Eberle et al., 2004; Horton et al., 2002; Ishii et al., 2004). The gene expression changes, with increased expression of *ChREBPβ* (a *ChREBPα* target), but not *Srebp1c* itself, in BA-DGAT-KO mice suggest activation of the ChREBP pathway, possibly accentuated by increased glucose uptake. Indeed, these findings are consistent with glucose-mediated activation of the MLX family of transcription factors (Kawaguchi et al., 2001; Ma et al., 2005), including ChREBP, and target genes that promote *de novo* lipogenesis in BAT (Mottillo et al., 2014; Sanchez-Gurmaches et al., 2018; Trayhurn, 1979; Yu et al., 2002). These findings are also consistent with increased expression of ChREBP/MLX-target genes in cells lacking LDs through DGAT inhibition (Mejhert et al., 2020). Activation of *de novo* lipogenesis in BAT is not strictly required for thermogenesis under normal conditions, however, as deletion of FA synthase in BAT is not essential for cold-induced thermogenesis (Guilherme et al., 2018); whether lipogenesis is essential in the BA-DGAT-KO model that lacks TG stores in brown adipocytes is unknown.

Previous studies also suggested a feedback mechanism correlating reduced DGAT activity with inhibition of the SREBP1-mediated lipogenic pathway (Chitraju et al., 2019; Choi et al., 2007; Monetti et al., 2007). This feedback response was not evident in BAT of BA-DGAT-KO mice. It is possible that lipids mediating SREBP-1 suppression in DGAT deficiency do not accumulate because of their consumption as fuel for thermogenesis. FAs were reduced in BAT of BA-DGAT-KO mice under thermogenic stimuli, perhaps because of enhanced use for fuel.

Finally, our studies highlight the use of glucose as a fuel for thermogenesis in rodents. We found dramatic changes in glucose uptake in BAT of BA-DGAT-KO mice, and these mice were protected from glucose intolerance when challenged with an HFD. These findings are consistent with other studies that illustrate that glucose disposal in brown adipocytes can protect against glucose intolerance peripherally (Chondronikola et al., 2014; Lee et al., 2014; Stanford et al., 2013). Thus, inhibition of

TG storage in BAT (or, by extrapolation, in brite/beige adipocytes) of humans could be metabolically beneficial in settings of insulin resistance.

## STAR★METHODS

Detailed methods are provided in the online version of this paper and include the following:

- **KEY RESOURCES TABLE**
- **RESOURCE AVAILABILITY**
  - Lead Contact
  - Materials Availability
  - Data and Code Availability
- **EXPERIMENTAL MODEL AND SUBJECT DETAILS**
  - Generation of BA-DGAT KO Mice
  - Mouse Husbandry
  - Cold Exposure Studies
- **METHOD DETAILS**
  - Metabolic Tracer Studies
  - [<sup>18</sup>F]-FDG-PET/CT Analysis
  - RNA Extraction and Quantitative Real-Time PCR (qRT-PCR)
  - Immunoblotting
  - Tissue Lipid Analysis
  - Isolation of Mitochondria from Brown Adipose Tissue
  - Isolation of Membrane Fraction from Brown Adipose Tissue
  - Glycogen Synthase Activity Assay
  - Respiration Analysis
  - Comprehensive Lab Animal Monitoring System (CLAMS)
- **QUANTIFICATION AND STATISTICAL ANALYSIS**

## SUPPLEMENTAL INFORMATION

Supplemental Information can be found online at <https://doi.org/10.1016/j.celrep.2020.108348>.

## ACKNOWLEDGMENTS

We thank members of the Farese & Walther laboratory for helpful comments, G. Howard for editorial assistance, and the Longwood small animal imaging facility at Beth Israel Deaconess Medical Center for PET/CT analysis. We thank Karen Inouye and Sarah Mitchell for helping with indirect calorimetry analysis. This work was supported in part by NIH grant R01 DK124913. T.C.W. is an investigator of the Howard Hughes Medical Institute. A.W.F. received support from the German Research Council (DFG) (FI 2476/1-1).

## AUTHOR CONTRIBUTIONS

C.C., R.V.F., and T.C.W. planned the study and designed the experiments. C.C. generated DGAT double flox and BA-DGAT-KO mice. C.C. performed most of the experiments. A.W.F. analyzed mitochondrial respiration and performed western blots of isolated mitochondria. C.C., R.V.F., and T.C.W. wrote the manuscript.

## DECLARATION OF INTERESTS

T.C.W. has an immediate family member working for Pfizer, Inc. T.C.W. and R.V.F. have a sponsored research agreement with Pfizer, Inc.

Received: April 30, 2020

Revised: August 29, 2020

Accepted: October 13, 2020

Published: November 3, 2020

## REFERENCES

- Bartelt, A., Bruns, O.T., Reimer, R., Hohenberg, H., Ittrich, H., Peldschus, K., Kaul, M.G., Tromsdorf, U.I., Weller, H., Waurisch, C., et al. (2011). Brown adipose tissue activity controls triglyceride clearance. *Nat. Med.* *17*, 200–205.
- Bartelt, A., Widenmaier, S.B., Schleim, C., Johann, K., Goncalves, R.L.S., Eguchi, K., Fischer, A.W., Parlakgul, G., Snyder, N.A., Nguyen, T.B., et al. (2018). Brown adipose tissue thermogenic adaptation requires Nrf1-mediated proteasomal activity. *Nat. Med.* *24*, 292–303.
- Bertholet, A.M., and Kirichok, Y. (2019). The mechanism FA-dependent H(+) transport by UCP1. *Handb. Exp. Pharmacol.* *251*, 143–159.
- Bertholet, A.M., Kazak, L., Chouchani, E.T., Bogaczynska, M.G., Paranjpe, I., Wainwright, G.L., Betourne, A., Kajimura, S., Spiegelman, B.M., and Kirichok, Y. (2017). Mitochondrial patch clamp of beige adipocytes reveals UCP1-positive and UCP1-negative cells both exhibiting futile creatine cycling. *Cell Metab.* *25*, 811–822.e4.
- Cannon, B., and Nedergaard, J. (2004). Brown adipose tissue: function and physiological significance. *Physiol. Rev.* *84*, 277–359.
- Cases, S., Smith, S.J., Zheng, Y.W., Myers, H.M., Lear, S.R., Sande, E., Novak, S., Collins, C., Welch, C.B., Lusis, A.J., et al. (1998). Identification of a gene encoding an acyl CoA:diacylglycerol acyltransferase, a key enzyme in triacylglycerol synthesis. *Proc. Natl. Acad. Sci. U S A* *95*, 13018–13023.
- Cases, S., Stone, S.J., Zhou, P., Yen, E., Tow, B., Lardizabal, K.D., Voelker, T., and Farese, R.V., Jr. (2001). Cloning of DGAT2, a second mammalian diacylglycerol acyltransferase, and related family members. *J. Biol. Chem.* *276*, 38870–38876.
- Chitraju, C., Mejhert, N., Haas, J.T., Diaz-Ramirez, L.G., Grueter, C.A., Imbriglio, J.E., Pinto, S., Koliwad, S.K., Walther, T.C., and Farese, R.V., Jr. (2017). Triglyceride synthesis by DGAT1 protects adipocytes from lipid-induced ER stress during lipolysis. *Cell Metab.* *26*, 407–418.e3.
- Chitraju, C., Walther, T.C., and Farese, R.V., Jr. (2019). The triglyceride synthesis enzymes DGAT1 and DGAT2 have distinct and overlapping functions in adipocytes. *J. Lipid Res.* *60*, 1112–1120.
- Choi, C.S., Savage, D.B., Kulkarni, A., Yu, X.X., Liu, Z.X., Morino, K., Kim, S., Distefano, A., Samuel, V.T., Neschen, S., et al. (2007). Suppression of diacylglycerol acyltransferase-2 (DGAT2), but not DGAT1, with antisense oligonucleotides reverses diet-induced hepatic steatosis and insulin resistance. *J. Biol. Chem.* *282*, 22678–22688.
- Chondronikola, M., Volpi, E., Borsheim, E., Porter, C., Annamalai, P., Enerback, S., Lidell, M.E., Saraf, M.K., Labbe, S.M., Hurren, N.M., et al. (2014). Brown adipose tissue improves whole-body glucose homeostasis and insulin sensitivity in humans. *Diabetes* *63*, 4089–4099.
- Chouchani, E.T., Kazak, L., and Spiegelman, B.M. (2019). New advances in adaptive thermogenesis: UCP1 and beyond. *Cell Metab.* *29*, 27–37.
- de Meis, L. (2003). Brown adipose tissue Ca<sup>2+</sup>-ATPase: uncoupled ATP hydrolysis and thermogenic activity. *J. Biol. Chem.* *278*, 41856–41861.
- Eberle, D., Hegarty, B., Bossard, P., Ferre, P., and Foulfelle, F. (2004). SREBP transcription factors: master regulators of lipid homeostasis. *Biochimie* *86*, 839–848.
- Fedorenko, A., Lishko, P.V., and Kirichok, Y. (2012). Mechanism of fatty-acid-dependent UCP1 uncoupling in brown fat mitochondria. *Cell* *151*, 400–413.
- Fischer, A.W., Shabalina, I.G., Mattsson, C.L., Abreu-Vieira, G., Cannon, B., Nedergaard, J., and Petrovic, N. (2017). UCP1 inhibition in Cidea-overexpressing mice is physiologically counteracted by brown adipose tissue hyperrecruitment. *Am. J. Physiol. Endocrinol. Metab.* *312*, E72–E87.
- Guilherme, A., Pedersen, D.J., Henriques, F., Bedard, A.H., Henchey, E., Kelly, M., Morgan, D.A., Rahmouni, K., and Czech, M.P. (2018). Neuronal modulation

- of brown adipose activity through perturbation of white adipocyte lipogenesis. *Mol. Metab.* **16**, 116–125.
- Hajdich, E., Aledo, J.C., Watts, C., and Hundal, H.S. (1997). Proteolytic cleavage of cellubrevin and vesicle-associated membrane protein (VAMP) by tetanus toxin does not impair insulin-stimulated glucose transport or GLUT4 translocation in rat adipocytes. *Biochem. J.* **321**, 233–238.
- Hankir, M.K., and Klingenspor, M. (2018). Brown adipocyte glucose metabolism: a heated subject. *EMBO Rep.* **19**, e46404.
- Hao, G., Du, Y., Zhou, X.J., Guo, J., Sun, X., Mohan, C., and Oz, O.K. (2013). Serial non-invasive assessment of antibody induced nephritis in mice using positron emission tomography. *PLoS ONE* **8**, e57418.
- Heine, M., Fischer, A.W., Schlein, C., Jung, C., Straub, L.G., Gottschling, K., Mangels, N., Yuan, Y., Nilsson, S.K., Liebscher, G., et al. (2018). Lipolysis triggers a systemic insulin response essential for efficient energy replenishment of activated brown adipose tissue in mice. *Cell Metab.* **28**, 644–655.e4.
- Himms-Hagen, J., Cui, J., Danforth, E., Jr., Taatjes, D.J., Lang, S.S., Waters, B.L., and Claus, T.H. (1994). Effect of CL-316,243, a thermogenic beta 3-agonist, on energy balance and brown and white adipose tissues in rats. *Am. J. Physiol.* **266**, R1371–R1382.
- Horton, J.D., Goldstein, J.L., and Brown, M.S. (2002). SREBPs: activators of the complete program of cholesterol and fatty acid synthesis in the liver. *J. Clin. Invest.* **109**, 1125–1131.
- Ishii, S., Iizuka, K., Miller, B.C., and Uyeda, K. (2004). Carbohydrate response element binding protein directly promotes lipogenic enzyme gene transcription. *Proc. Natl. Acad. Sci. U S A* **101**, 15597–15602.
- Kawaguchi, T., Takenoshita, M., Kabashima, T., and Uyeda, K. (2001). Glucose and cAMP regulate the L-type pyruvate kinase gene by phosphorylation/dephosphorylation of the carbohydrate response element binding protein. *Proc. Natl. Acad. Sci. U S A* **98**, 13710–13715.
- Kazak, L., Chouchani, E.T., Jedrychowski, M.P., Erickson, B.K., Shinoda, K., Cohen, P., Vetrivelan, R., Lu, G.Z., Laznik-Bogoslavski, D., Hasenfuss, S.C., et al. (2015). A creatine-driven substrate cycle enhances energy expenditure and thermogenesis in beige fat. *Cell* **163**, 643–655.
- Koliwad, S.K., Streeper, R.S., Monetti, M., Cornelissen, I., Chan, L., Terayama, K., Naylor, S., Rao, M., Hubbard, B., and Farese, R.V., Jr. (2010). DGAT1-dependent triacylglycerol storage by macrophages protects mice from diet-induced insulin resistance and inflammation. *J. Clin. Invest.* **120**, 756–767.
- Kong, X., Banks, A., Liu, T., Kazak, L., Rao, R.R., Cohen, P., Wang, X., Yu, S., Lo, J.C., Tseng, Y.H., et al. (2014). IRF4 is a key thermogenic transcriptional partner of PGC-1 $\alpha$ . *Cell* **158**, 69–83.
- Lass, A., Zimmermann, R., Haemmerle, G., Riederer, M., Schoiswohl, G., Schweiger, M., Kienesberger, P., Strauss, J.G., Gorkiewicz, G., and Zechner, R. (2006). Adipose triglyceride lipase-mediated lipolysis of cellular fat stores is activated by CGI-58 and defective in Chanarin-Dorfman Syndrome. *Cell Metab.* **3**, 309–319.
- Lee, P., Smith, S., Linderman, J., Courville, A.B., Brychta, R.J., Dieckmann, W., Werner, C.D., Chen, K.Y., and Celi, F.S. (2014). Temperature-acclimated brown adipose tissue modulates insulin sensitivity in humans. *Diabetes* **63**, 3686–3698.
- Listenberger, L.L., Han, X., Lewis, S.E., Cases, S., Farese, R.V., Jr., Ory, D.S., and Schaffer, J.E. (2003). Triglyceride accumulation protects against fatty acid-induced lipotoxicity. *Proc. Natl. Acad. Sci. U S A* **100**, 3077–3082.
- Liu, L., Trent, C.M., Fang, X., Son, N.H., Jiang, H., Blanner, W.S., Hu, Y., Yin, Y.X., Farese, R.V., Jr., Homma, S., et al. (2014). Cardiomyocyte-specific loss of diacylglycerol acyltransferase 1 (DGAT1) reproduces the abnormalities in lipids found in severe heart failure. *J. Biol. Chem.* **289**, 29881–29891.
- Lowell, B.B., and Spiegelman, B.M. (2000). Towards a molecular understanding of adaptive thermogenesis. *Nature* **404**, 652–660.
- Luijten, I.H.N., Brooks, K., Boulet, N., Shabalina, I.G., Jaiprakash, A., Carlsson, B., Fischer, A.W., Cannon, B., and Nedergaard, J. (2019). Glucocorticoid-induced obesity develops independently of UCP1. *Cell Rep.* **27**, 1686–1698.e5.
- Ma, L., Tsatsos, N.G., and Towle, H.C. (2005). Direct role of ChREBP.Mix in regulating hepatic glucose-responsive genes. *J. Biol. Chem.* **280**, 12019–12027.
- Mejhert, N., Kuruvilla, L., Gabriel, K.R., Elliott, S.D., Guie, M.A., Wang, H., Lai, Z.W., Lane, E.A., Christiano, R., Danial, N.N., et al. (2020). Partitioning of MLX-family transcription factors to lipid droplets regulates metabolic gene expression. *Mol. Cell* **77**, 1251–1264.e9.
- Mills, E.L., Pierce, K.A., Jedrychowski, M.P., Garrity, R., Winther, S., Vidoni, S., Yoneshiro, T., Spinelli, J.B., Lu, G.Z., Kazak, L., et al. (2018). Accumulation of succinate controls activation of adipose tissue thermogenesis. *Nature* **560**, 102–106.
- Monetti, M., Levin, M.C., Watt, M.J., Sajan, M.P., Marmor, S., Hubbard, B.K., Stevens, R.D., Bain, J.R., Newgard, C.B., Farese, R.V., Sr., et al. (2007). Dissociation of hepatic steatosis and insulin resistance in mice overexpressing DGAT in the liver. *Cell Metab.* **6**, 69–78.
- Mottillo, E.P., Balasubramanian, P., Lee, Y.H., Weng, C., Kershaw, E.E., and Granneman, J.G. (2014). Coupling of lipolysis and de novo lipogenesis in brown, beige, and white adipose tissues during chronic beta3-adrenergic receptor activation. *J. Lipid Res.* **55**, 2276–2286.
- Periasamy, M., Maurya, S.K., Sahoo, S.K., Singh, S., Sahoo, S.K., Reis, F.C.G., and Bal, N.C. (2017). Role of SERCA pump in muscle thermogenesis and metabolism. *Compr. Physiol.* **7**, 879–890.
- Sanchez-Gurmaches, J., Tang, Y., Jespersen, N.Z., Wallace, M., Martinez Callejman, C., Gujja, S., Li, H., Edwards, Y.J.K., Wolfrum, C., Metallo, C.M., et al. (2018). Brown fat AKT2 is a cold-induced kinase that stimulates ChREBP-mediated de novo lipogenesis to optimize fuel storage and thermogenesis. *Cell Metab.* **27**, 195–209.e6.
- Schreiber, R., Diwoky, C., Schoiswohl, G., Feiler, U., Wongsiriroj, N., Abdellatif, M., Kolb, D., Hoeks, J., Kershaw, E.E., Sedej, S., et al. (2017). Cold-induced thermogenesis depends on ATGL-mediated lipolysis in cardiac muscle, but not brown adipose tissue. *Cell Metab.* **26**, 753–763.e7.
- Schweiger, M., Schreiber, R., Haemmerle, G., Lass, A., Fledelius, C., Jacobsen, P., Tornqvist, H., Zechner, R., and Zimmermann, R. (2006). Adipose triglyceride lipase and hormone-sensitive lipase are the major enzymes in adipose tissue triacylglycerol catabolism. *J. Biol. Chem.* **281**, 40236–40241.
- Shabalina, I.G., Petrovic, N., de Jong, J.M., Kalinovich, A.V., Cannon, B., and Nedergaard, J. (2013). UCP1 in brite/beige adipose tissue mitochondria is functionally thermogenic. *Cell Rep.* **5**, 1196–1203.
- Shih, M.Y., Kane, M.A., Zhou, P., Yen, C.L., Streeper, R.S., Napoli, J.L., and Farese, R.V., Jr. (2009). Retinol Esterification by DGAT1 Is Essential for Retinoid Homeostasis in Murine Skin. *J. Biol. Chem.* **284**, 4292–4299.
- Shin, H., Ma, Y., Chanturiya, T., Cao, Q., Wang, Y., Kadegowda, A.K.G., Jackson, R., Rumore, D., Xue, B., Shi, H., et al. (2017). Lipolysis in brown adipocytes is not essential for cold-induced thermogenesis in mice. *Cell Metab.* **26**, 764–777.e5.
- Smith, R.E., and Roberts, J.C. (1964). Thermogenesis of brown adipose tissue in cold-acclimated rats. *Am. J. Physiol.* **206**, 143–148.
- Smith, R.E., Roberts, J.C., and Hittelman, K.J. (1966). Nonphosphorylating respiration of mitochondria from brown adipose tissue of rats. *Science* **154**, 653–654.
- Stanford, K.I., Middelbeek, R.J., Townsend, K.L., An, D., Nygaard, E.B., Hitchcox, K.M., Markan, K.R., Nakano, K., Hirshman, M.F., Tseng, Y.H., et al. (2013). Brown adipose tissue regulates glucose homeostasis and insulin sensitivity. *J. Clin. Invest.* **123**, 215–223.
- Teperino, R., Amann, S., Bayer, M., McGee, S.L., Loipetzberger, A., Connor, T., Jaeger, C., Kammerer, B., Winter, L., Wiche, G., et al. (2012). Hedgehog partial agonism drives Warburg-like metabolism in muscle and brown fat. *Cell* **151**, 414–426.
- Townsend, K.L., and Tseng, Y.H. (2014). Brown fat fuel utilization and thermogenesis. *Trends Endocrinol. Metab.* **25**, 168–177.
- Trayhurn, P. (1979). Fatty acid synthesis in vivo in brown adipose tissue, liver and white adipose tissue of the cold-acclimated rat. *FEBS Lett.* **104**, 13–16.

- Tschop, M.H., Speakman, J.R., Arch, J.R., Auwerx, J., Bruning, J.C., Chan, L., Eckel, R.H., Farese, R.V., Jr., Galgani, J.E., Hambly, C., et al. (2011). A guide to analysis of mouse energy metabolism. *Nat. Methods* 9, 57–63.
- Virtue, S., Feldmann, H., Christian, M., Tan, C.Y., Masoodi, M., Dale, M., Lelliott, C., Burling, K., Campbell, M., Eguchi, N., et al. (2012). A new role for lipocalin prostaglandin D synthase in the regulation of brown adipose tissue substrate utilization. *Diabetes* 61, 3139–3147.
- Wayllace, N.Z., Valdez, H.A., Meras, A., Ugalde, R.A., Busi, M.V., and Gomez-Casati, D.F. (2012). An enzyme-coupled continuous spectrophotometric assay for glycogen synthases. *Mol. Biol. Rep.* 39, 585–591.
- Wu, J., Bostrom, P., Sparks, L.M., Ye, L., Choi, J.H., Giang, A.H., Khandekar, M., Virtanen, K.A., Nuutila, P., Schaart, G., et al. (2012). Beige adipocytes are a distinct type of thermogenic fat cell in mouse and human. *Cell* 150, 366–376.
- Yen, C.L., Stone, S.J., Koliwad, S., Harris, C., and Farese, R.V., Jr. (2008). Thematic review series: glycerolipids. DGAT enzymes and triacylglycerol biosynthesis. *J. Lipid Res.* 49, 2283–2301.
- Yoneshiro, T., Wang, Q., Tajima, K., Matsushita, M., Maki, H., Igarashi, K., Dai, Z., White, P.J., McGarrah, R.W., Ilkayeva, O.R., et al. (2019). BCAA catabolism in brown fat controls energy homeostasis through SLC25A44. *Nature* 572, 614–619.
- Yu, X.X., Lewin, D.A., Forrest, W., and Adams, S.H. (2002). Cold elicits the simultaneous induction of fatty acid synthesis and beta-oxidation in murine brown adipose tissue: prediction from differential gene expression and confirmation in vivo. *FASEB J.* 16, 155–168.
- Zechner, R., Zimmermann, R., Eichmann, T.O., Kohlwein, S.D., Haemmerle, G., Lass, A., and Madeo, F. (2012). FAT SIGNALS—lipases and lipolysis in lipid metabolism and signaling. *Cell Metab.* 15, 279–291.

STAR★METHODS

KEY RESOURCES TABLE

REAGENT or RESOURCE	SOURCE	IDENTIFIER
<b>Antibodies</b>		
Rabbit monoclonal anti-Glut1	Cell Signaling Technology	Cat#12939
Mouse monoclonal anti-Glut4	Cell Signaling Technology	Cat# 2213
Rabbit polyclonal anti- Na, K-ATPase	Cell Signaling Technology	Cat# 3010
Rabbit polyclonal anti-tyrosine hydroxylase	Abcam	Cat# ab112
Rabbit monoclonal anti-Akt	Cell Signaling Technology	Cat# 4691
Rabbit monoclonal anti-phospho-Akt (Ser473)	Cell Signaling Technology	Cat# 4060
Rabbit polyclonal anti-AMPK $\alpha$	Cell Signaling Technology	Cat# 2532
Rabbit monoclonal anti-phospho-AMPK $\alpha$ (Thr172)	Cell Signaling Technology	Cat# 2535
Rabbit polyclonal anti-UCP1	Abcam	Cat# ab10983
Total OXPHOS Rodent WB Antibody Cocktail	Abcam	Cat# ab110413
Rabbit polyclonal anti-PGDS	Abcam	Cat# ab182784
Rabbit monoclonal anti-GAPDH	Cell Signaling Technology	Cat# 5174S
Mouse monoclonal anti- $\alpha$ -Tubulin	Sigma-Aldrich	Cat# T9026
<b>Chemicals, Peptides and Recombinant Proteins</b>		
1,2-Dioleoyl-rac-glycerol	Sigma-Aldrich	Cat# D8394
Oleoyl coenzyme A lithium salt	Sigma-Aldrich	Cat# O1012
Oleoyl [14C] Coenzyme A	American Radiolabeled Chemicals, Inc.	Cat# ARC 0527
Oleic acid [14C]	American Radiolabeled Chemicals, Inc.	Cat# ARC 0297
Thin Layer Chromatography Plates	Analtech	Cat# P43911
Insulin	Lilly Corporation	Humulin R (U 100)
CL 316,243 hydrate	Sigma-Aldrich	Cat# C5976
Glycogen from bovine liver	Sigma-Aldrich	Cat# G0885
Protease inhibitors	Roche	Cat# 11873580001
Phospho(enol)pyruvic acid monopotassium salt	Sigma-Aldrich	Cat# P7127
Pyruvate Kinase from rabbit muscle	Sigma-Aldrich	Cat# P1506
$\beta$ -Nicotinamide adenine dinucleotide	Sigma-Aldrich	Cat# N8129
<b>Critical Commercial Assays</b>		
Power SYBR Green PCR Master Mix	Life Technologies	Cat # 4368706
iScript cDNA Synthesis Kit	Biorad	Cat # 170-8891
RNeasy Mini Kit	QIAGEN	Cat # 74106
QIAzol Lysis Reagent	QIAGEN	Cat # 79306
QIAshredder	QIAGEN	Cat# 79656
RNase-Free DNase Set	QIAGEN	Cat# 79254
SuperSignal West Pico	ThermoFisher Scientific	Cat# 34580
SuperSignal West Femto	ThermoFisher Scientific	Cat# 34095
Glycogen Assay Kit II	Abcam	Cat# ab169558
Infinity Triglycerides Reagent	Thermo Fisher	Cat # TR22421
Infinity Cholesterol Reagent	Thermo Fisher	Cat # TR13421
Free Glycerol Reagent	Sigma-Aldrich	Cat # F6428
HR Series NEFA-HR(2) Color Reagent A	FUJIFILM Medical Systems	Cat # 999-34691
HR Series NEFA-HR(2) Solvent A	FUJIFILM Medical Systems	Cat # 995-34791

(Continued on next page)

**Continued**

REAGENT or RESOURCE	SOURCE	IDENTIFIER
HR Series NEFA-HR(2) Color Reagent B	FUJIFILM Medical Systems	Cat # 991-34891
HR Series NEFA-HR(2) Solvent B	FUJIFILM Medical Systems	Cat # 993-35191
Experimental Models: Organisms/ Strains		
Dgat1 <sup>flox/flox</sup> mice	(Shih et al., 2009); The Jackson Laboratory	Cat # 017322
Dgat2 <sup>flox/flox</sup> mice	(Chitraju et al., 2019); The Jackson Laboratory	Cat # 033518
Ucp1-Cre mice	(Kong et al., 2014); The Jackson Laboratory	Cat # 024670
BA-DGAT KO mice	This paper	N/A
Other		
Chow-diet	PicoLab® Rodent Diet 20	Cat # 5053
Breeder's-diet	PicoLab® Rodent Diet 20	Cat # 5058
High-fat-diet	Envigo	Cat # TD.88137

**RESOURCE AVAILABILITY**

**Lead Contact**

Further information and requests for resources and reagents should be directed to and will be fulfilled by the Lead Contact Tobias C. Walther ([twalther@hsph.harvard.edu](mailto:twalther@hsph.harvard.edu)).

**Materials Availability**

Mouse models generated in this study are available from the Lead Contact Tobias C. Walther ([twalther@hsph.harvard.edu](mailto:twalther@hsph.harvard.edu)) upon completion of a material transfer agreement.

**Data and Code Availability**

This study did not generate any unique dataset or code.

**EXPERIMENTAL MODEL AND SUBJECT DETAILS**

**Generation of BA-DGAT KO Mice**

To generate BAT-specific *Dgat1* and *Dgat2* double knockout (BA-DGAT KO) mice, we first generated *Dgat1* and *Dgat2* double-floxed mice (D1D2 flox) by crossing *Dgat1*<sup>flox/flox</sup> mice (Shih et al., 2009) (The Jackson Laboratory stock number: 017322) with *Dgat2*<sup>flox/flox</sup> mice (Chitraju et al., 2019) (The Jackson Laboratory stock number: 033518). To generate BA-DGAT KO mice, we crossed D1D2 flox mice with transgenic mice expressing Cre recombinase under control of the murine *Ucp1* promoter (Kong et al., 2014) (The Jackson Laboratory stock number: 024670).

**Mouse Husbandry**

All mouse experiments were performed under the guidelines from Harvard Center for Comparative Medicine. Mice were maintained in a barrier facility, at room temperatures (22–23°C), on a regular 12-h light and 12-h dark cycle and had *ad libitum* access to food and water unless otherwise stated. Mice were fed on standard laboratory chow diet (PicoLab® Rodent Diet 20, 5053; less than 4.5% crude fat) or Western-type high-fat diet (Envigo, TD.88137; 21.2% fat by weight, 42% kcal from fat). For all our experiments mice aged 12–14 weeks were used. For high-fat-diet feeding studies both male and female mice were used, for all remaining experiments male mice were used.

**Cold Exposure Studies**

For cold exposure experiments (at 4°C), mice were single-housed in the morning around 8:00 am. Mice had free access to food and water unless otherwise stated. Hourly core body temperatures were recorded using a rectal probe thermometer.

**METHOD DETAILS**

**Metabolic Tracer Studies**

Mice were housed in cages without food for 1 h before the start of the experiment. β-3 adrenergic receptor agonist (CL 316,243) was administered via injection (intraperitoneal injection, 1 mg/kg body weight). Control mice were given saline injections. After 1 h of CL 316,243 injection, mice were intraperitoneally-administered with [<sup>3</sup>H]-deoxyglucose (2 μCi/g bodyweight) or [<sup>14</sup>C]-oleic acid (0.5 μCi/g bodyweight) conjugated with bovine serum albumin. At 1 h after tracer injection, mice were sacrificed by decapitation, and tissues

were collected. Tissues were lysed in lysis buffer (250 mM sucrose, 50 mM Tris Cl, pH 7.4, with protease inhibitor cocktail (11873580001, Roche)). Radioactivity in tissue lysates was measured by liquid scintillation counting.

### **[<sup>18</sup>F]-FDG-PET/CT Analysis**

PET/CT imaging studies were performed on a Siemens Inveon PET/CT Multimodality System (Hao et al., 2013). In brief, mice were fasted for 1 h before the experiment. CL 316,243 was administered via injection (intraperitoneal injection, 1 mg/kg body weight). 1 h after CL 316,243 injection, an intravenous injection of [<sup>18</sup>F]-FDG was made into the tail. Subsequently, the mouse was placed onto the imaging bed under 2% isoflurane anesthesia for the duration of imaging. After acquiring CT images at 80 kV and 500 mA with a focal spot of 58 mm, with a binning factor of 1:x, a whole-body PET scan was acquired. Co-registration of the reconstructed CT and PET images and image analysis were done using the manufacturer's software. For PET quantification, the regions of interest (ROI) were selected using CT images as guides.

### **RNA Extraction and Quantitative Real-Time PCR (qRT-PCR)**

Total RNA from brown and white adipose tissues was isolated with the Qiazol lysis reagent and using the protocol of the RNeasy Kit (QIAGEN). Complementary DNA was synthesized using the iScript cDNA Synthesis Kit (Bio-Rad), and qPCRs were performed using the SYBR Green PCR Master Mix Kit (Applied Biosystems). Primers used in this study are listed in supplemental information (Table S2).

### **Immunoblotting**

Tissues were lysed using RIPA lysis buffer (25 mM Tris Cl pH 7.6, 150 mM NaCl, 1% NP-40, 1% sodium deoxycholate, 0.1% SDS) containing protease inhibitors (11873580001, Roche). Proteins were denatured in Laemmli buffer and were separated on 10% SDS-PAGE gels, and transferred to PVDF membranes (Bio-Rad). The membranes were blocked with blocking buffer for 1 h in TBST containing 5% BSA or 5% milk, and then incubated with primary antibodies overnight. The membranes were then washed three times with TBST for 10 min, and incubated in mouse secondary antibodies (Santa Cruz Biotechnology) at 1:5000 dilutions in blocking buffer. Membranes were washed again three times with TBST for 10 min, and revealed using the Super Signal West Pico kit (Thermo Scientific).

### **Tissue Lipid Analysis**

Brown adipose tissue was homogenized in 1 mL of lysis buffer (250 mM sucrose, 50 mM Tris Cl, pH 7.0 with protease inhibitor cocktail (11873580001, Roche)). The homogenate was mixed with 5 mL of chloroform:methanol (3:2 v/v) and extracted for 2 h by vigorous shaking. Upon centrifugation at 3000 x g at room temperature for 10 min, 100  $\mu$ l of lower organic phase was collected and dried in a speed vac. To the dried lipids, 100–300  $\mu$ l of 0.1% Triton X-100 was added and the solution was sonicated using ultrasonic homogenizer (Biologics, Inc., model 3000MP) for 10 s. with 30% amplitude. The total TG content was measured using the Infinity TM triglycerides reagent (Thermo Scientific) according to the manufacturer's protocol. For plasma lipid measurements, 5  $\mu$ l of plasma was used.

### **Isolation of Mitochondria from Brown Adipose Tissue**

Mitochondria were isolated from brown adipose tissue as described (Fischer et al., 2017; Luijten et al., 2019; Shabalina et al., 2013). Briefly, iBAT and scBAT of two mice was pooled in ice-cold isolation buffer (250 mM sucrose buffer, 5 mM Tris Cl pH 7.4, 2 mM EGTA, 2% BSA). Tissues were minced, further homogenized in a glass homogenizer with six strokes, filtered through cotton gauze and centrifuged at 8500 x g (JA-2550, Beckmann) for 10 min. The supernatant was discarded by inverting the tube, the pellet was resuspended in isolation buffer, homogenized in a glass homogenizer and centrifuged at 800 x g for 10 min. The supernatant, containing mitochondria, was centrifuged at 8500 x g for 10 min, and the mitochondrial pellet was resuspended in TES buffer (100 mM KCl, 20 mM TES, 1 mM EGTA, 0.6% BSA, pH 7.2) to induce mitochondrial swelling. After centrifugation at 8500 x g for 10 min, the supernatant was discarded and the mitochondria were resuspended in the remaining TES buffer. The solution was transferred to a small glass homogenizer, homogenized and the protein concentration was determined.

### **Isolation of Membrane Fraction from Brown Adipose Tissue**

Plasma membrane fraction was isolated as previously described (Hajduch et al., 1997). Brown adipose tissue was homogenized in ice-cold Tris-sucrose buffer (50 mM Tris Cl, pH 7.4, 250 mM sucrose, with protease inhibitors (11873580001, Roche)) in Dounce-glass homogenizer. The homogenate was centrifuged at 16000 x g for 15 min. The supernatant (S1) was retained on ice. The pellet from this spin was re-suspended in Tris-sucrose buffer and was gently homogenized and layered over a 1.2 M sucrose cushion and centrifuged at 100,000 x g for 70 min. Plasma membrane fraction from this spin were recovered from the top of the sucrose cushion and diluted in Tris-sucrose buffer and re-pelleted by centrifugation at 45000 x g for 45 min.

### **Glycogen Synthase Activity Assay**

The spectrophotometric determination of *in vitro* glycogen synthase activity was performed as described previously (Wayllace et al., 2012). The reaction buffer contained 50 mM Bicine, pH 8.0, 80 mM MnCl<sub>2</sub>, 0.4 mM NADH, 1 mM phosphoenolpyruvate, 1 U lactate

dehydrogenase, 1 U pyruvate kinase, 10 mg of rabbit muscle glycogen and 3.5 mM ADPGlc. When UDPGlc was used as glycosyl donor, the medium contained 50 mM Bicine, pH 8.0, 80 mM MnCl<sub>2</sub>, 0.4 mM NADH, 1 mM phosphoenolpyruvate, 1 U lactate dehydrogenase, 1 U pyruvate kinase, 1 U adenylate kinase, 5 mM ATP, 10 mg of rabbit muscle glycogen and 20 mM UDPGlc. The final volume of each reaction was 400  $\mu$ l. Glycogen synthase activity was measured by following the oxidation of NADH to NAD. NADH levels were quantified by absorbance at 340 nm.

### Respiration Analysis

Respiration analysis was performed in a Seahorse XF96 analyzer (Agilent), as described before ([Bartelt et al., 2018](#)) with some modifications. A total of 5  $\mu$ g mitochondrial protein in 20  $\mu$ l TES buffer per well was loaded into Agilent Seahorse XF96 cell culture microplates and mitochondria were pelleted by centrifugation at 4000  $\times$  g for 15 min. Respiration was measured in respiration media (100 mM KCl, 20 mM TES, 1 mM EGTA, 2 mM MgCl<sub>2</sub>, 1 mM KH<sub>2</sub>PO<sub>4</sub>, 0.5 mM CaCl<sub>2</sub>, 0.5% BSA, pH 7.2) containing substrate (20 mM glycerol-3-phosphate, 10 mM succinate + 5  $\mu$ M rotenone or 5 mM pyruvate + 3 mM malate). UCP1-dependent respiration was blocked by addition of 5 mM GDP (Port A), and UCP1-dependent respiration was calculated by subtracting the respiration values after GDP-addition from basal uncoupled respiration in the presence of substrate. ATP-production was stimulated by addition of 1 mM ADP (Port B) and inhibited by addition of 1  $\mu$ M oligomycin (Port C). ATP-synthesis activity was calculated by subtracting the respiration levels after oligomycin addition from the respiration levels after ADP addition. Mitochondrial respiration was then inhibited by addition of 1  $\mu$ M antimycin A and 1  $\mu$ M rotenone (Port D). The results from five independent mitochondrial preparations per genotype (mice housed at room temperature) were used for analysis with at least 8 technical replicates per isolation and condition. For the calculation of the total mitochondrial yield, the protein concentration in the mitochondrial preparations was multiplied with the total volume. For western blot analysis, 20  $\mu$ g of protein were separated on 4%–15% SDS-PAGE, transferred onto PVDF-membranes in a wet-blotting system.

### Comprehensive Lab Animal Monitoring System (CLAMS)

Mice were housed individually, and acclimatized for two days. Oxygen consumption, carbon dioxide release, energy expenditure, and activity were measured using a Columbus Instruments' Oxymax Comprehensive Lab Animal Monitoring System (CLAMS) system according to guidelines for measuring energy metabolism in mice ([Tschop et al., 2011](#)).

### QUANTIFICATION AND STATISTICAL ANALYSIS

Data are presented as mean  $\pm$  SD (standard deviation). Statistical significance was evaluated by unpaired two-tailed Student's t test or two-way ANOVA with Bonferroni's multiple comparison test. Statistically significant differences are annotated as follows: \*p < 0.05, \*\*p < 0.01, \*\*\*p < 0.001, \*\*\*\*p < 0.0001

**Cell Reports, Volume 33**

**Supplemental Information**

**Lipid Droplets in Brown Adipose Tissue**

**Are Dispensable for Cold-Induced Thermogenesis**

**Chandramohan Chitraju, Alexander W. Fischer, Robert V. Farese Jr., and Tobias C. Walther**

## Supplementary Figure 1

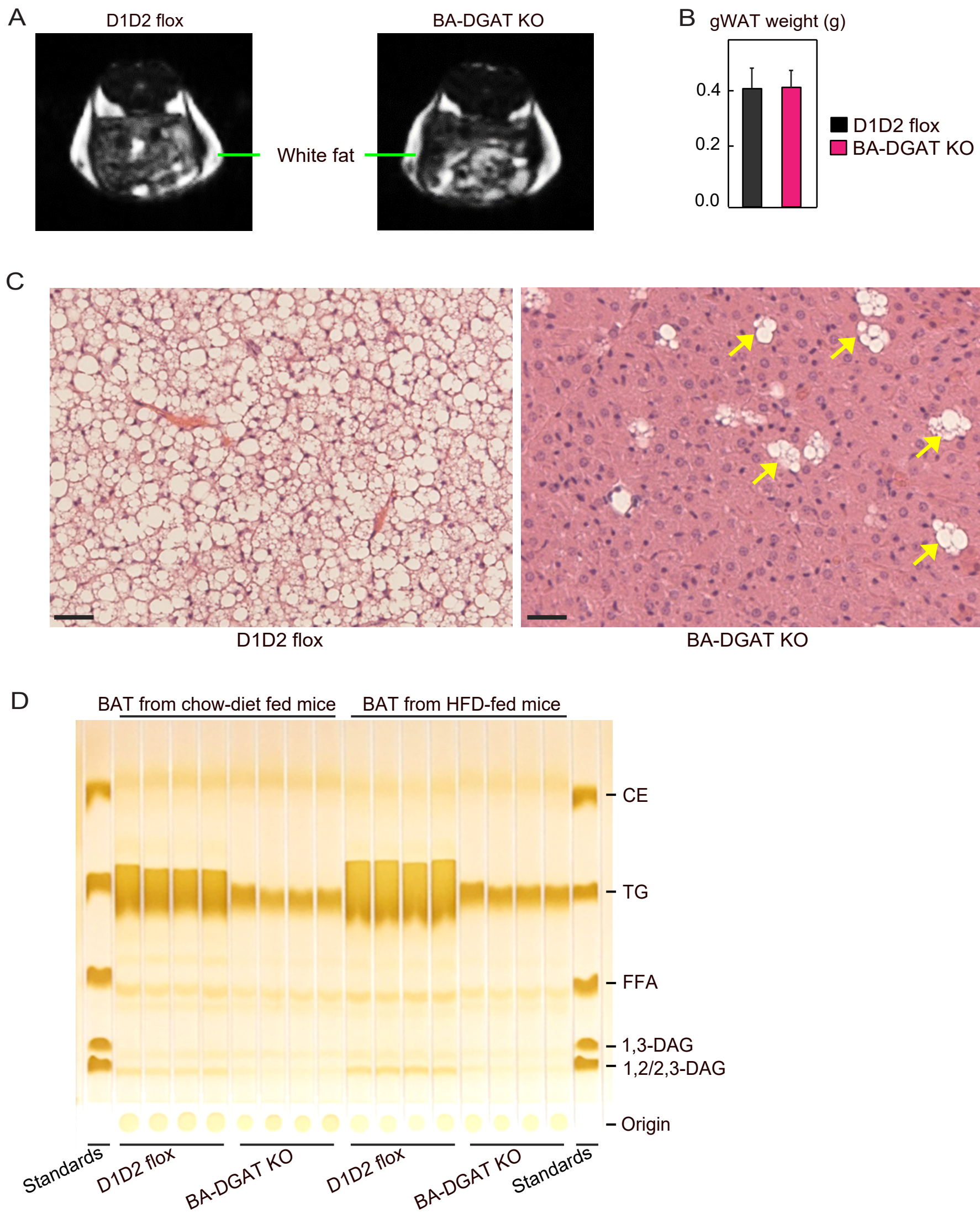


**Figure S1. Related to Figure 1. Fat mass Analysis of BA-DGAT KO Mice and Thin Layer Chromatography Analysis of Neutral Lipids from BAT.**

(A) Nuclear magnetic resonance imaging (MRI) scans of D1D2 flox and BA-DGAT KO mice (n=3).

(B) Weights of gonadal fat depots from chow-diet-fed mice (n=6).

(C) H&E-stained sections of BAT. LDs were absent in nearly all cells of BAT depots in BA-DGAT KO mice. A few cells of unknown identity (arrow heads) in BAT of BA-DGAT KO mice still had LDs. Scale bars, 50  $\mu$ m.

(D) Thinlayer chromatography analysis of neutral lipids extracted from BAT. Triglycerides present in BAT of BA-DGAT KO mice account for few cells of unknown identity that still had LDs. CE, cholesterol esters; TG, triglycerides; FFA, free fatty acids; DAG, diacyl glycerol. (n=4). Lipids loaded onto TLC were normalized to proteins.

Data are presented as mean  $\pm$  SD. \*\*\*p<0.001 by t-test.

Supplementary Figure 2

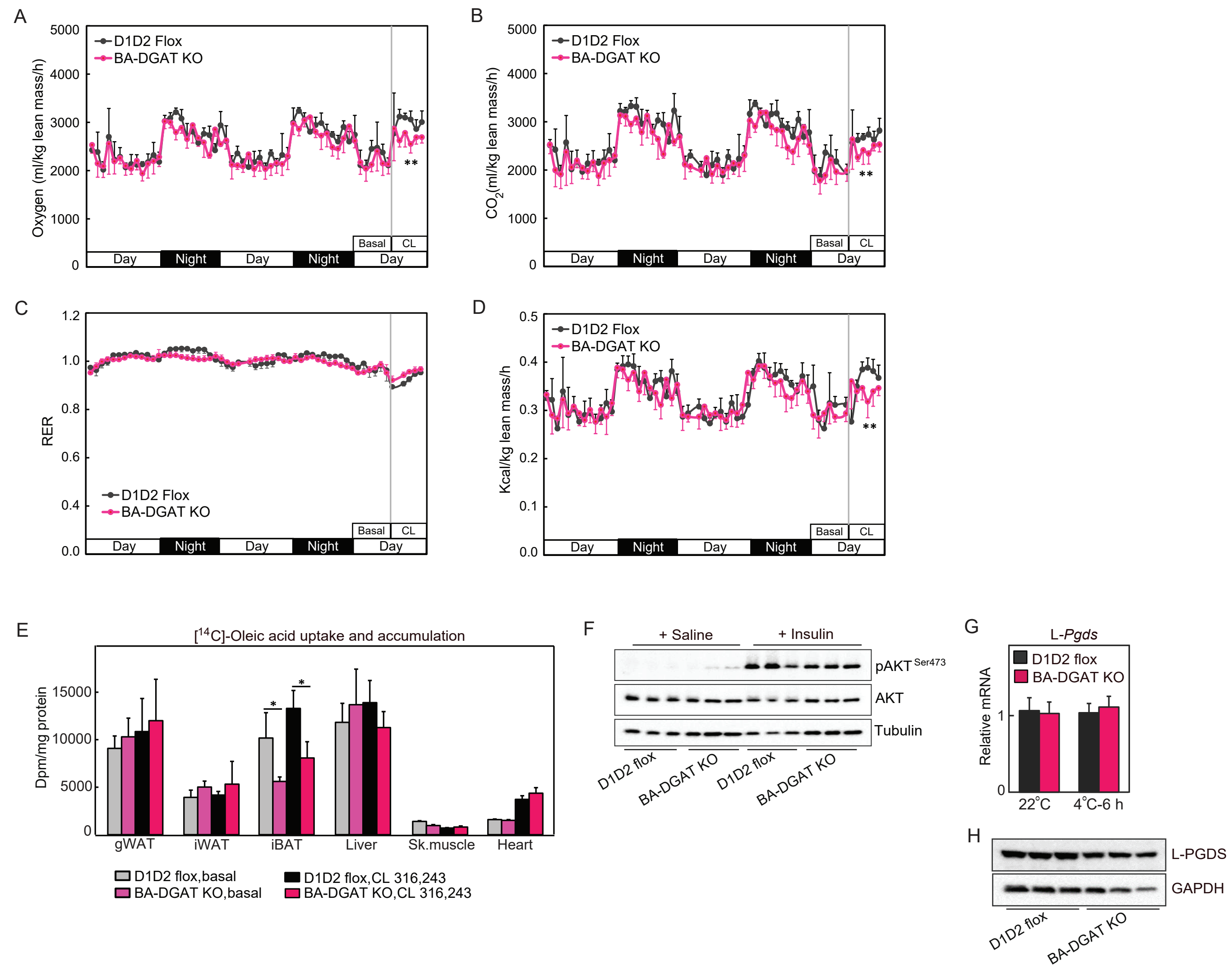


**Figure S2. Related to Figures 2 and 3. Analysis of Insulin signalling in BAT and Indirect calorimetry analysis of BA-DGAT KO mice.**

(A-D) Oxygen consumption, carbon dioxide release, energy expenditure and RER in basal or CL 316,243-administered mice. Each data point represents the mean of six readings per hour (n=4).

(E) [14C]-oleic acid uptake by tissues in basal or in CL 316,243-administered mice (n=3).

(F) Western blot analysis of insulin signaling in BAT of basal or insulin-administered mice (n=3).

(G) mRNA levels of *L-Pgds* in BAT of mice housed at room temperature (22°C) or cold exposed for 6 hours (4°C-6h) (n=6).

(H) Immunoblot analysis of L-PGDS in BAT of mice housed at room temperature (n=3).

Data are presented as mean ± SD. \*p<0.05, \*\*p<0.01.

Supplementary Figure 3

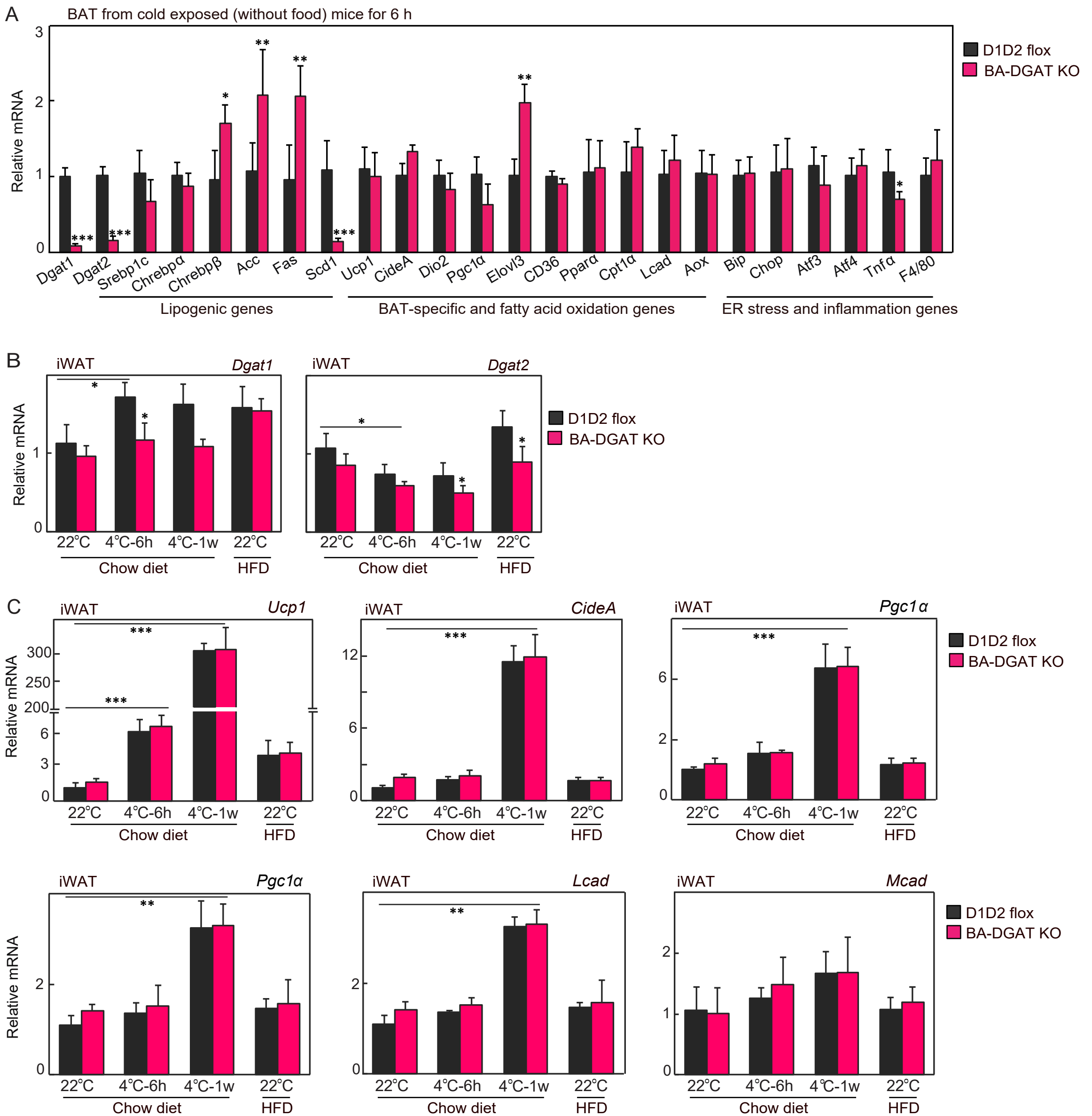


**Figure S3. Related to Figure 3. Quantitative Real-Time PCR Analysis of genes in BAT and iWAT.**

(A) mRNA levels in BAT of cold exposed (without food) mice for 6 hours (n=6).

(B) *Dgat1* and *Dgat2* mRNA levels in iWAT of acutely or chronically cold exposed or high-fat-diet fed mice (n=6).

(C) mRNA levels of thermogenic genes in iWAT of acutely or chronically cold exposed or high-fat-diet fed mice (n=6).

Data are presented as mean ± SD. \*p<0.05, \*\*p<0.01, \*\*\*p<0.001.

## Supplementary Figure 4

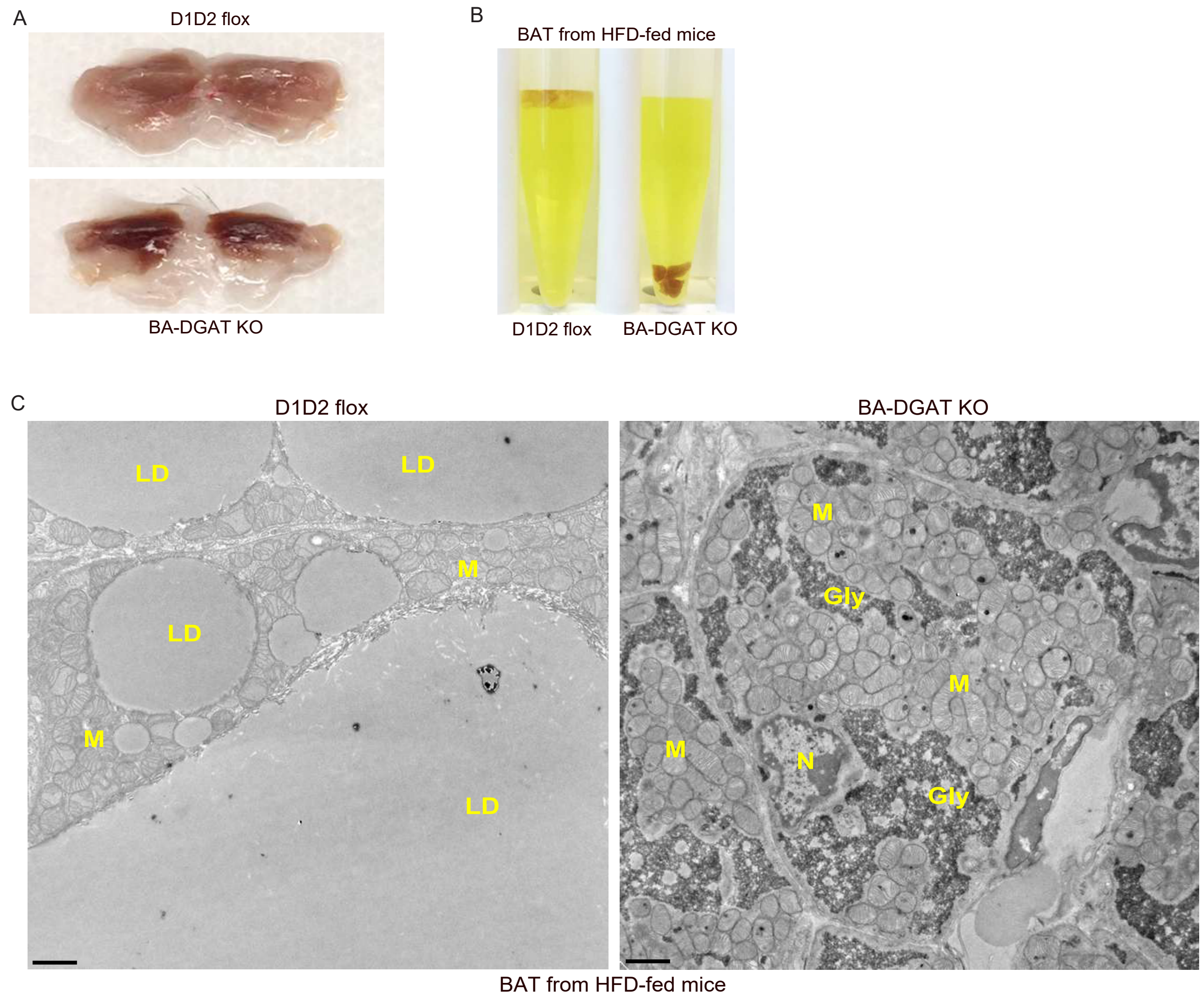


**Figure S4. Related to Figure 4. Gross Appearance of BAT and TEM images of BAT from HFD-fed mice.**

(A) Gross appearance of BAT from 12 weeks HFD-fed mice.

(B) BAT of HFD-fed BA-DGAT KO mice sinks in an aqueous buffer with fixative (1.25% formaldehyde, 2.5 % glutaraldehyde and 0.03% picric acid in 0.1 M sodium cacodylate buffer, pH 7.4, density of the fixative is 1.01 g/ml) used to fix BAT tissue for electron microscopy.

(C) TEM images of BAT from 12 weeks HFD-fed mice; scale bars, 2  $\mu$ m. LD, lipid droplet; M, mitochondria; N, nucleus; Gly, glycogen.

### Supplementary Table S1. Related to Figure 1

Plasma metabolites from *ad libitum* chow diet fed mice

Plasma metabolites	D1D2 flox	BA-DGAT KO
Glucose (mg/dl)	158 ± 9.5	146 ± 8.5*
Free fatty acids (m mol/l)	0.42 ± 0.09	0.41 ± 0.07
Free glycerol (m mol/l)	0.17 ± 0.06	0.19 ± 0.03
Triglycerides (mg/dl)	41 ± 8.8	31 ± 4.5*
Total cholesterol (mg/dl)	88 ± 18	77 ± 10
Insulin (ng/ml)	0.61 ± 0.07	0.59 ± 0.05

(n=8-11 mice) values are mean ± SD. \*p<0.05

## Supplementary Table S2. Related to STAR Method RNA Extraction and Quantitative Real-Time PCR

Primers used for quantitative Real-Time PCR analysis of mouse genes

Gene	Primer sequence (5'-3')
<i>Cyclophilin</i>	Fwd: GGAGATGGCACAGGAGGAAA Rev: CCGTAGTGCTTCAGTTTGAAGTTCT
<i>Dgat1</i>	Fwd: GGAATATCCCCGTGCACAA Rev: CATTGCTGCTGCCATGTC
<i>Dgat2</i>	Fwd: CCGCAAAGGCTTTGTGAA Rev: GGAATAAGTGGGAACCAGATCAG
<i>Glut1</i>	Fwd: GGCCAGATTCATCAACTGGAT Rev: GCTCCAAGGCTGTACCCTAAG
<i>Glut4</i>	Fwd: GTGACTGGAACACTGGTCCTA Rev: CCAGCCAGTTGCATTGTAG
<i>Glycogen synthase</i>	Fwd: GAACGCAGTGCTTTTCGAGG Rev: CCAGATAGTAGTTGTCAACCCAT
<i>Glycogenin</i>	Fwd: TGGAGTCTTTGTCTATCAACCCT Rev: TTGCCAGCCACTAAAATATGT
<i>Sreb1c</i>	Fwd: GGAGCCATGGATTGCACATT Rev: GGCCCGGAAGTCACTGT
<i>Chrebpa</i>	Fwd: CGACACTCACCCACCTCTTC Rev: TTGTTCCAGCCGGATCTTGTC
<i>Chrebpβ</i>	Fwd: TCTGCAGATCGCGTGGAG Rev: CTTGTCCCGGCATAGCAAC
<i>Fas</i>	Fwd: GGAGGTGGTGATAGCCGGTAT Rev: TGGGTAATCCATAGAGCCCAG
<i>Acc</i>	Fwd: GATGAACCATCTCCGTTGGC Rev: GACCCAATTATGAATCGGGAGTG
<i>Elovl3</i>	Fwd: TTCTCACGCGGGTTAAAAATGG Rev: GAGCAACAGATAGACGACCAC
<i>Scd1</i>	Fwd: TTCTTGCGATACACTCTGGTGC Rev: CGGGATTGAATGTTCTTGTCGT
<i>Ucp1</i>	Fwd: AGGCTTCCAGTACCATTAGGT Rev: CTGAGTGAGGCAAAGCTGATTT
<i>CideA</i>	Fwd: TGCTCTTCTGTATCGCCCAGT Rev: GCCGTGTTAAGGAATCTGCTG
<i>Dio2</i>	Fwd: CAGTGTGGTGCACGTCTCCAATC Rev: TGAACCAAAGTTGACCACCAG
<i>Pgc1α</i>	Fwd: TTCATCTGAGTATGGAGTCGCT Rev: GGGGGTGAAACCACTTTTGTA
<i>Ppara</i>	Fwd: AATGCAATTTCGCTTTGGAAG Rev: GGCCTTGACCTTGTTTCATGT
<i>Cpt1α</i>	Fwd: GAACCCCAACATCCCCAAAC Rev: TCCTGGCATTGTCCTGGAAT
<i>Mcad</i>	Fwd: AGGTTTCAAGATCGCAATGG Rev: CTCCTTGGTGCTCCACTAGC
<i>Lcad</i>	Fwd: TCCATGGCAAATACTGGGC Rev: TTGCAATCGGGTACTCCAC
<i>Aox</i>	Fwd: CTCATCTTCGAGGCTTGAAACCAC Rev: ATTTACGGATAGGGACAAGAAAGGC
<i>Cd36</i>	Fwd: ATGGGCTGTGATCGGAACTG Rev: GTCTTCCAATAAGCATGTCTCC
<i>Bip</i>	Fwd: ACTTGGGGACCACCTATTCTT Rev: ATCGCCAATCAGACGCTCC
<i>Chop</i>	Fwd: CCACCACACCTGAAAGCAGAA Rev: AGGTGAAAGGCAGGGACTCA
<i>Atf3</i>	Fwd: GAGGATTTTGCTAACCTGACACC Rev: TTGACGGTAACTGACTCCAGC
<i>Atf4</i>	Fwd: CCTTCGACCAGTCGGGTTTG Rev: CTGTCCCAGAAAAGGCATCC
<i>Cd68</i>	Fwd: TGTCTGATCTTGCTAGGACCG Rev: GAGAGTAACGGCCTTTTGTGA
<i>Tnfa</i>	Fwd: CCCTCACACTCAGATCATCTTCT Rev: GCTACGACGTGGGCTACAG
<i>F4/80</i>	Fwd: TGACTCACCTTGTGGTCCTAA Rev: CTTCCAGAATCCAGTCTTTCC
<i>L-Pgds</i>	Fwd: GACAAGTTTCTGGGGCGCTGGT Rev: GCTGTAGAGGGTGGCCATGCGG

Fwd, forward; Rev, reverse.